UNCERTAIN INTERVAL SYSTEMS WITH APPLICATION TO SEPARATELY EXCITED DC MOTOR AND DC-DC CONVERTERS

by

NARENDRA KINTALI

A dissertation submitted in partial fulfillment of the
requirements for the degree of

DOCTOR OF PHILOSOPHY IN ELECTRICAL AND COMPUTER ENGINEERING

2024

Oakland University
Rochester, Michigan

Doctoral Advisory Committee:

Ka C. Cheok, Ph.D., Chair
Aycil Cesmelioglu, Ph.D.
Daniel Llamocca, Ph.D.
Brian P. Sangeorzan, Ph.D.

ACKNOWLEDGMENTS

I would like to express my deepest gratitude to my advisor, Prof. Ka C. Cheok, for his unwavering support, patience, and insightful guidance throughout my doctoral journey. His positive criticism and expertise have been invaluable in shaping this dissertation, and his encouragement has kept me motivated even during challenging times.

I am also profoundly grateful to the members of my Doctoral Advisory Committee for their time and constructive criticism which greatly improved the quality of this research. A heartfelt thanks to Meghana, Murali and my friends for their unconditional love, patience, and understanding during this challenging period. Their support has been a constant source of motivation.

Lastly, I would like to acknowledge the financial support and resources provided by the university, which made my journey easy.

Thank you all for contributing to the successful completion of this dissertation.

Narendra Kintali

ABSTRACT

UNCERTAIN INTERVAL SYSTEMS WITH APPLICATION TO SEPARATELY EXCITED DC MOTOR AND DC-DC CONVERTERS

by

NARENDRA KINTALI

Adviser: Ka C. Cheok, Ph.D.

Electric drive systems in automobiles, aircraft, and maritime crafts have significantly advanced due to changes in hardware and software applications. Drive systems consisting of multidisciplinary subsystems often post non-trivial control problems that must be overcome. For example, redundant input systems related to a separately excited DC motor (SEDCM) or highly varying gains related to DC-DC converters.

This thesis introduces a novel approach utilizing an optimization scheme to transform the redundant input process into an uncertain interval system. An armature voltage minimization scheme was developed for the SEDCM to address these redundancies and uncertainties. The comprehensive analysis and feedback control design for an uncertain interval optimal redundant input system is a significant departure from traditional methods, such as Root Locus. The Kharitonov stability criterion is used to analyze the interval systems and determine the parameter boundaries for the controller gains. At the same time, the Root-Locus method is employed to visualize the stable

regions of the controller parameters. Next, the Lyapunov stability criterion-based adaptive controller is designed to guarantee stability and tracking for the optimal redundant input systems. For illustration, a PI-controlled separately excited DC motor (SEDCM) will be used.

The proposed uncertain interval technique is extended to analyze and design a robust PI controller for DC-DC power electronic converters. The results unify the control design for the buck, boost, and buck-boost converters.

TABLE OF CONTENTS

LIST OF TABLES

LIST OF FIGURES

LIST OF FIGURES-continued

LIST OF FIGURES-continued

CHAPTER ONE

INTRODUCTION

1.1 Separately Excited Direct Current Motors

SEDCM, which is a type of DC motor, has advantages, drawbacks, and areas for improvement. SEDCM offers precise speed control, making it suitable for applications requiring accurate speed regulation. These motors can achieve high-efficiency levels, especially when matched with advanced control systems. SEDCMs are versatile and find applications in various industries, including robotics, manufacturing, and electric vehicles and they exhibit good dynamic response characteristics, making them suitable for applications where rapid changes in speed are required.

SEDCMs may have limitations in terms of scalability to higher power levels compared to alternative motor types. It's important to note that advancements in electric motors, including SEDCMs, continue to be an active area of research and development.

1.2 DC Motors and Optimization Techniques

Prior work has focused on energy optimal control schemes [12], energy saving using recursive linear least square algorithm [13], and other AI-based controlled design techniques [14-17]. Such research has largely been focused on controller design or optimization [18], whereas this thesis focuses on both Armature and Field voltage, as well as current optimization and system stability, using Kharitonov's theorem, providing a timely addition to the current body of literature.

1.3 DC-DC Converters

Buck-boost converters and H-bridge circuits are both common electronic circuits used in power electronics, but they serve different purposes and have distinct configurations. The primary purpose of a buck-boost converter is to provide a regulated output voltage that can be either higher or lower than the input voltage. It can step up (boost) or step down (buck) the voltage. It typically consists of a single inductor, a switch (transistor), a diode, and a capacitor. The switching action of the transistor allows the converter to regulate the output voltage. During the switching cycle, energy is stored in the inductor when the switch is closed and released to the output when the switch is open, allowing for voltage conversion. This process provides a regulated output voltage, even when the input voltage varies. A system like this is commonly used in battery-powered devices, solar power systems, and applications where input voltage can vary.

1.4 Organization of Chapters

Chapter two of the dissertation provides details for executing a differentiation-based optimization technique to minimize both the armature and field voltage of an SEDCM and compares current requirements for developing desired torque in a motor with and without optimization.

Chapter three of the dissertation describes interval transfer function implementation using Matlab Simulink, explains Kharitonov's stability analysis through the Root-Locus method, and explores the stability boundaries of uncertain systems using Kharitonov's criterion.

Chapter four of this dissertation presents the design and implementation method of an adaptive controller for nonlinear uncertain systems using Lyapunov stability criterion. The proposed controller is developed using Matlab and applied to a Separately Excited Direct Current motor (SEDCM) to achieve the desired speed.

Chapter five of the dissertation discusses a transfer function-based controller technique for DC-DC converters using a DC transfer function. It is developed and simulated in Matlab to demonstrate its effectiveness.

1.5 Contributions

The contributions of the thesis are the novel unified approaches comprising the following:

- Posing particular non-trivial control problems as uncertain interval control systems. These include the dual redundant input SEDCM and rapidly varying gain DC-DC converters.
- Minimizing the armature and field currents of an SEDCM and transforming a non-linear redundant system to an uncertain interval system.
- Complementing Kharitonov stability analysis with Root Locus plot to yield stable region for proportional-integral (PI) controller parameters.
- Design and implementation of Direct Lyapunov Adaptive Control (DLAC) to control the speed of the motor of uncertain interval SEDCM systems.
- Formulation of buck, boost, and buck-boost DC-DC converters as uncertain interval systems.
- Development of robust PI control design method for near-instantaneous tracking responses for DC converters.

- Implementation of theoretical insights and numerical examples as illustrated via Matlab, Simulink, and Simscape. The novel comprehensive approach can be applied to non-trivial problems related to electric drives and other practical situations.

CHAPTER TWO

NON-LINEAR MODELS OF AN OPTIMAL REDUNDANT-INPUT SYSTEM

2.1 Introduction to SEDCM

Fast response, simple control requirements and precise control over wide bandwidth make DC motors desirable, while Permanent Magnet DC (PMDC) motors provide better controllability and efficiency[1] but magnetic field of PMDC cannot be varied. Whereas series and shunt DC motors applications are limited because Armature and Field currents independent control is not possible. In SEDCM these drawbacks can be overruled, and with precise combination of Armature and Field voltages various possible speed vs torque characteristic drive can be implemented.

Electrical Equivalent circuit of SEDCM is as shown in Fig. 2.1. Based on Kirchoff's voltage law, the equations governing the armature circuit and field circuit are given as below[1]-[2]. The variables and parameters are defined in Table 2.1.

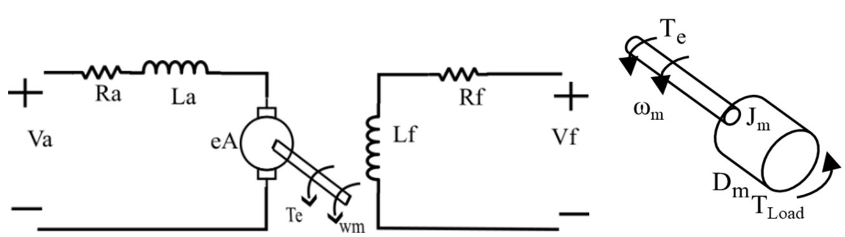

Figure 2.1: Electrical Equivalent circuit of SEDCM with Load

$$V_a = R_a i_a + L_a \frac{di_a}{dt} + e_A \ , \qquad 2.1$$

$$V_f = R_f i_f + L_f \frac{di_f}{dt} \ , \qquad 2.2$$

where $e_A = K_v \phi \omega_m$.

Based on Newton's Law of Motion

$$T_e = J_m \frac{d\omega_m}{dt} + D_m \omega_m + T_{load} \quad , \qquad 2.3$$

where $T_e = K_t \phi i_a$ and $\phi = f(i_f)$.

Setting the time derivative of the equations to zero, steady-state equations can be derived. In steady state the torque vs speed relation can be given as.

$$\begin{aligned} T_{Load} &= -D_m \omega_m + T_e \\ &= -\left(D_m + \frac{K_t K_v \phi^2}{R_a} \right) \omega_m + K_t \phi \left(\frac{V_a}{R_a} \right) \end{aligned} \qquad 2.4$$

2.2 Optimization Algorithm

The rise in computational power of microprocessors, when combined with optimization techniques - algorithms for maximum drive with least amount of energy usage can be developed for a motor. One such minimization technique is presented in this paper for a SEDCM. To establish this optimization framework, the governing equations are derived from the electrical equivalent circuit of the motor and the hysteresis behavior of currents[2].

Optimizing voltage and current not only improves the efficiency of the motor but also the performance[3]. Optimized armature current leads to reduced losses like core losses and stray-load losses[4-5].

2.2.1 Minimization of V_a and hence i_a

Substituting e_A and T_e in eq 2.1 during steady state. (in steady state $\frac{di_a}{dt} = 0$ and $\frac{di_f}{dt} = 0$),

$$V_a = R_a i_a + e_A = R_a \frac{T_e}{K_t \phi} + K_v \phi \omega_m$$
$$= a\frac{1}{\phi} + b\phi \qquad 2.5$$

where $a = \frac{R_a T_e}{K_t}$ *and* $b = K_v \omega_m$.

From the above eq 2.5 it is evident that V_a is a function of Ø. Closed-from minimum can be found when derivative is equated to zero.

$$\frac{dV_a}{d\phi} = -a\frac{1}{\phi^2} + b = 0 \quad ,$$
$$\phi_1 = \sqrt{\frac{a}{b}} \qquad 2.6$$

For simplicity the speed of the motor is considered positive, making b > 0. Substituting eq 2.6 in eq 2.5.

$$V_{a,\min} = a\frac{1}{\phi_1} + b\phi_1 \qquad 2.7$$

The field winding magnetic flux $\phi = f(i_f)$ is a non-linear function with saturation and hysteresis. In the non-saturating region of $f(i_f)$, we can assume that $\phi = K_\phi i_f$ (where K_ϕ is a constant)

$$
\begin{aligned}
i_{f,1} &= f^{-1}(\phi_1) = \frac{1}{K_\phi}\phi_1 \quad , \\
V_{f,1} &= R_f i_{f,1}
\end{aligned} \qquad 2.8
$$

2.3 Matlab Implementation and Limitations

The verification optimization technique is done using Matlab Simulink. A SEDCM with the specifications mentioned in Table 2.1. is considered for this purpose. The following considerations are made for Simulink implementation, in eq 2.3 torque developed by the motor T_e is replaced with T_{des} desired torque, K_t and K_v are considered equal (K_t=K_V=K) and the load applied (T_{Load}) on the shaft is considered as zero [3] for simplicity.

Table 2.1 shows the values taken from the Matlab for different parameters, which are considered in simulating the equations.

Table 2.1: Motor specifications

Parameter and variables	**Value**
Armature voltage	V_a = 240 Volts
Armature resistance	R_a = 2.58 Ohms
Field voltage	V_f = 300 Volts
Field resistance	R_f = 281.2 Ohms
Armature inductance	L_a = 0.028 Henry
Field inductance	L_f= 156 Henry
Voltage constant	K_v = 1.8V/A rad
Inertia	J_m = 0.02215 Kg m^2
Damping	D_m = 0.02953 Nms/rad
Torque constant	K_t = 1.8 Nm/A^2
Flux constant	$K_Ø$ = 1

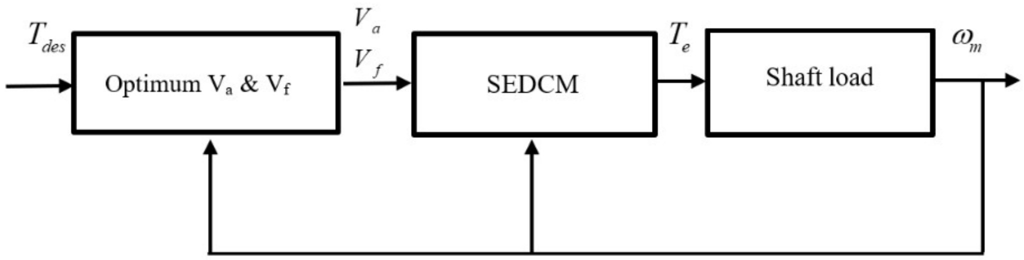

Equations for optimum V_a & V_f:	**Equations for SEDCM:**	**Equations for shaft load:**
$a = \frac{R_a T_{des}}{K}$ $b = K\,\omega_m$ $\phi_1 = \sqrt{\frac{a}{b}}$ $V_{a,1} = a\frac{1}{\phi_1} + b\phi_1$ $i_{f,1} = f^{-1}(\phi_1)$ $V_{f,1} = R_f i_{f,1}$	$L_f \frac{d\,i_f}{dt} = -R_f i_f + V_f$ $L_a \frac{d\,i_a}{dt} = -R_a i_a - e_A + V_a$ $\phi = f(i_F)$ $e_A = K\,\phi\,\omega_m$ $T_e = K\,\phi\,i_a$	$T_e = J_m \frac{d\omega_m}{dt} + D_m\omega_m$

Figure 2.2: Block diagram for MATLAB implementation

2.4 Results

From Fig 2.2, it is evident that the SEDCM with optimization algorithm produces desired torque under no load condition as shown in Fig. 2.3. Implementation is also successful when a non-zero load is applied on the model, as shown in Fig. 2.4. Fig. 2.5 shows how the speed varies with variation in the desired torque.

Table.3. Gives a comparison between the amount of voltage and current needed to develop a specific amount of torque from SEDCM with and without optimization. It is evident from the data that optimization algorithms reduce the amount of current needed to develop desired torque. When the current is reduced core losses in the motor reduces and efficiency increases.

Table 2.2: Voltage and Current requirements

Desired torque (Nm)		V_a **(V)**	V_f **(V)**	i_a **(A)**	i_f **(A)**	ω_m **(rad/sec)**
40	Optimization + SEDCM	748	78.6	144	0.28	1354
	SEDCM	750	80	148.5	0.29	1358
		748	78.6	150.7	0.28	1354
		760	70	170	0.25	1360
		785	60	197.7	0.21	1356
		790	50	234	0.18	1337
30	Optimization + SEDCM	560	78	108.2	0.28	1016
	SEDCM	560	80	110.9	0.29	1014
		560	78	113.6	0.28	1013
		575	70	128.6	0.25	1029
		590	60	148.7	0.21	1019
		640	50	180.4	0.18	1031
20	Optimization + SEDCM	373.8	78.6	72.0	0.28	675
	SEDCM	375	80	74.2	0.29	679
		373.8	78.6	75.3	0.28	676
		374	79	72.4	0.28	675
		380	60	97.8	0.21	656
		420	50	118.4	0.18	677

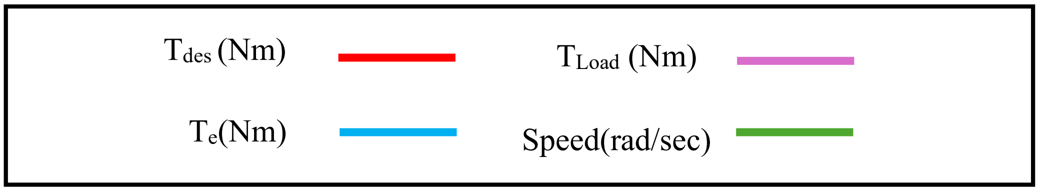

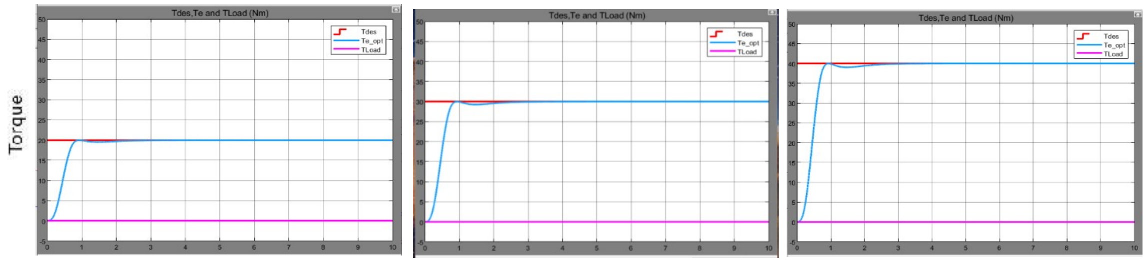

(a) (b) (c)

Figure 2.3: (a)T_{des} = 20Nm, T_e = 20Nm and T_{Load} = 0Nm. (b)T_{des} = 30Nm, T_e = 30Nm and T_{Load} = 0Nm. (c)T_{des} = 40Nm, T_e = 40Nm and T_{Load} = 0Nm.

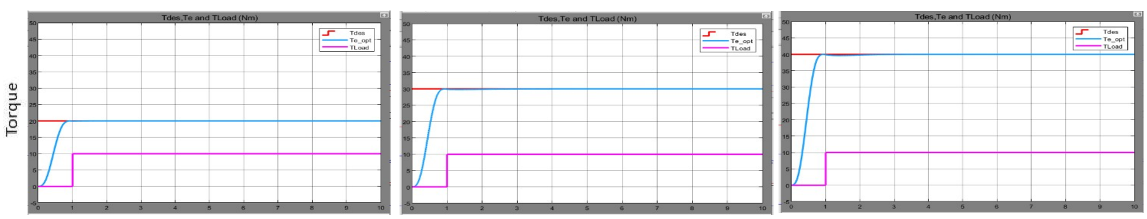

(a) (b) (c)

Figure 2.4: (a) T_{des} = 20Nm, T_e = 20Nm and T_{Load} = 10Nm. (b) T_{des} = 30Nm, T_e = 30Nm and T_{Load} = 10Nm. (c) T_{des} = 40Nm, T_e = 40Nm and T_{Load} = 10Nm.

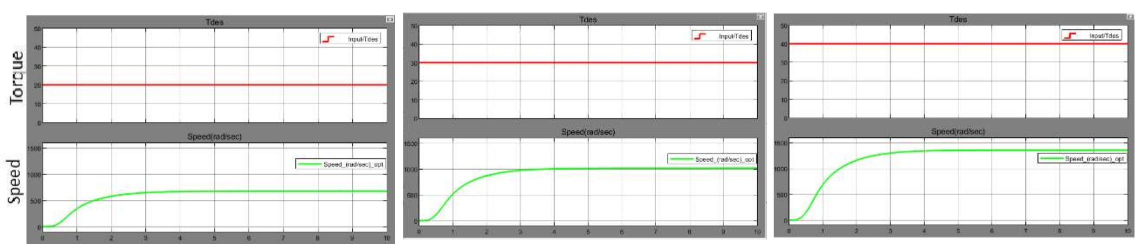

(a) (b) (c)

Figure 2.5: (a) T_{des} = 20Nm. (b) T_{des} = 30Nm (c) T_{des} = 40Nm.

CHAPTER THREE

INTERVAL SYSTEM STABILITY ANALYSIS WITH PI CONTROLLER

SEDCM, along with the optimization algorithm, is unstable because it consists of non-linearity functions and uncertain parameters Systems with non-linearity and uncertainty can be represented using interval transfer functions. Kharitonov's stability theorem [6,7,8] can then be used to analyze the stability of a feedback control interval system. Kharitonov's method generates four polynomials, each for numerator and denominator. The sixteen boundary transfer functions built using these polynomials are used for plotting stability boundary locus in the (k_p , k_i)-plane [9]. This method is also used for the design of PI, PID Controller. For simplicity, the PI controller was chosen for stability analysis. PI, PID and lead/lag controllers are widely used in industries.[10,11].

3.1 Interval System and Matlab Implementation

Transfer function of optimized SEDCM is found with the help of Matlab-*System Identification Toolbox's, tfest* [4] command. Consider the Desired torque as the input and the Speed of the SEDCM as the output of the transfer function. A number of zeros and poles of the transfer function can be regulated[4]. Table 3.1 Displays the transfer functions of the system in Fig. 2.2 with different T_{des} under no load.

In Table 3.1, the transfer functions in the third column with one zero and two poles are considered for discussion on the stability of the system. When T_{des} is 40Nm transfer function indicates there is no zero on the right-hand side of S-plane, whereas when T_{des} is 30Nm or 20 Nm there is a zero on the on the right-hand side of S-Plane. This indicates there is non-linearity because of variable torque. To build the controller for the system with non-linearity it is important to understand the stability of the system and because of huge deviations in coefficients of numerator and denominator values for different T_{des} interval system is built.

Table 3.1: Transfer functions with different number of poles and zeros

T_{des}	**First order transfer function** $G(s)$	**Second order transfer function** $G(s)$	**First order transfer function with delay** $G(s)$	**Second order transfer function with delay** $G(s)$
40	$\frac{31.38}{s+0.9277}$	$\frac{-26.27s+2945}{s^2+94.64s+86.6}$	$e^{-0.029s}\frac{31.43}{s+0.9242}$	$e^{-0.018s}\frac{-41.87s+6949}{s^2+222.1s+204.4}$
30	$\frac{31.74}{s+0.9377}$	$\frac{104.9s+3003}{s^2+95.41s+88.34}$	$e^{-0.029s}\frac{31.8}{s+0.9353}$	$e^{-0.017s}\frac{-41.31s+5931}{s^2+187.5s+174.5}$
20	$\frac{32.36}{s+0.9522}$	$\frac{113.7s+3048}{s^2+95.01s+89.7}$	$e^{-0.029s}\frac{32.41}{s+0.9539}$	$e^{-0.017s}\frac{-45.35s+6074}{s^2+188.4s+178.8}$
Based on upper and lower limits of T_{des}	$\frac{[32.3,31.4]}{s+[0.95,1]}$	$\frac{[114,-26.27]s+[3048,2945]}{s^2+[95,94.64]s+[90,86.6]}$	$e^{-0.029s}\frac{[32.4,31.43]}{s+[0.95,0.92]}$	$e^{-0.017s}\frac{[-45.35,-41.87]s+[6074,6949]}{s^2+[188.4,221]s+[178.8,204.4]}$

3.1.1 Non-Linear Plant Model

Matlab lacks native support for interval system transfer functions and nonlinear plant models. Consequently, an alternative approach leveraging Lookup Table (LUT) blocks within Simulink is suggested for the construction of an interval system transfer function. Given that the coefficient limits of the interval system transfer function are ascertainable, the development of a corresponding Simulink model can be accomplished by adhering to the mathematical framework outlined below.

Consider

$$\frac{d\omega_m(t)}{dt} \approx -a_o\,\omega_m(t) + b_o T_{des}(t), \quad a_o \in [\underline{a}_o, \overline{a}_o],\; b_o \in [\underline{b}_o, \overline{b}_o] \qquad 3.1$$

the transfer function for an uncertain interval system can be written as

$$\frac{\omega_m(s)}{T_{des}(s)} = G(s) = \frac{b_o}{s + a_o} \qquad 3.2$$

Drawing a comparison between the interval transfer function $\frac{[32.3,31.4]}{s+[0.95,1]}$ (from Table 3.1) and eq 3.1. the coefficients can be determined as follows.

$$b_0 \in [32.3,31.4]$$
$$a_0 \in [0.95,1]$$

The Simulink model shown below was built using interval system coefficients and Matlab.

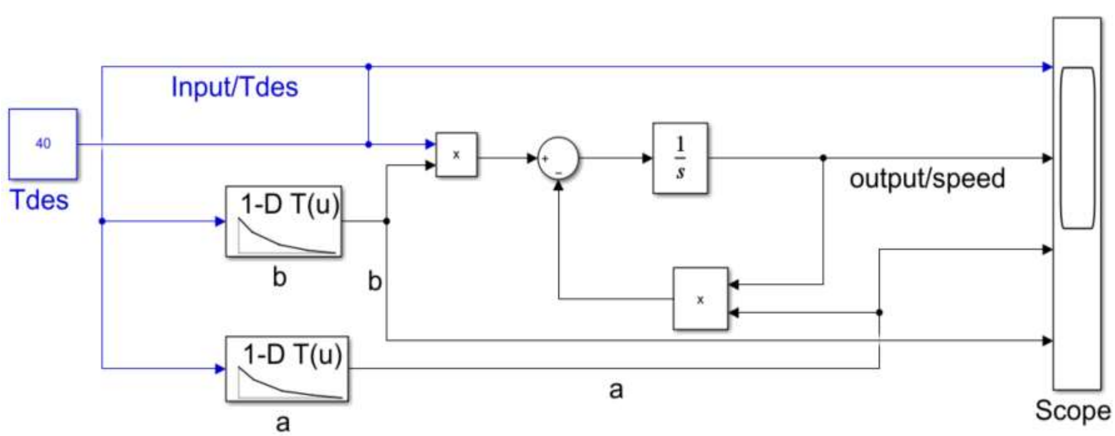

Figure 3.1: Matlab model built using LUT blocks of Simulink

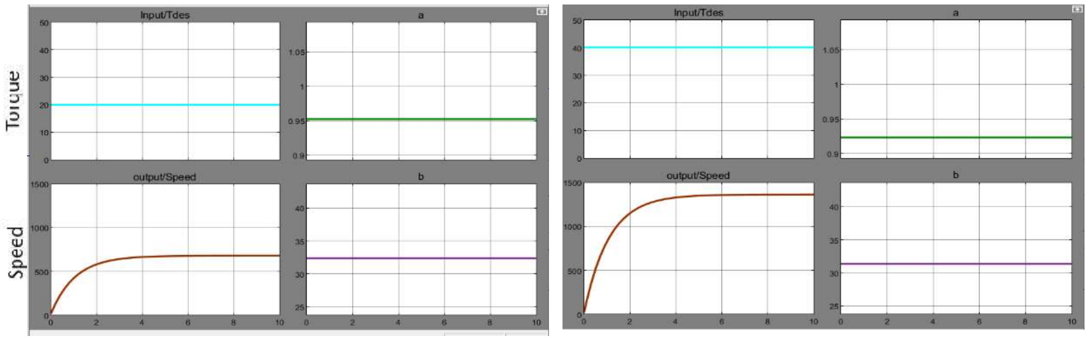

(a) (b)

Figure 3.2: (a)Tdes = 20Nm, (b)Tdes = 40Nm

Upon comparison of Fig 3.2(a,b) with Fig 2.5, a noteworthy observation emerges: the output speed remains consistent for a given input torque across scenarios. This similarity underscores a crucial inference—that the Simulink model, crafted through the incorporation of Look-Up Table (LUT) blocks, effectively simulates the behavior characteristic of an interval system transfer function. Thereby validating its efficacy in capturing the dynamic interplay between input torque and output speed within the specified system parameters.

3.2 Controller Design Scheme

Consider a unity feedback system with a PI controller and a plant, as shown in Fig 3.3. Where G(s) is the plant and C(s) is the controller[9].

$$G(s) = \frac{N(s)}{D(s)} \text{ and } C(s) = \frac{K_p s + K_i}{s}$$

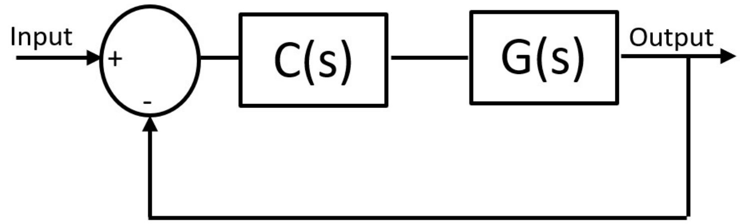

Figure 3.3: SISO control system

For explanation, G(s) chosen as third order system (three poles)

$$G(s) = \frac{b}{(s+p_1)(s+p_2)(s+p_3)} = \frac{b}{s^3 + a_1 s^2 + a_2 s + a_3} \quad 3.3$$

as compensator is a PI controller it has zero and a pole.

$$C(s) = K_p + \frac{K_i}{s} = \frac{K_p(s + \frac{K_i}{K_p})}{s} = \frac{K_p(s + Z_c)}{s} \quad 3.4$$

The closed loop transfer function of the considered unity feedback system is given by

$$\frac{G(s)C(s)}{1+G(s)C(s)} = \frac{\frac{b}{s^3 + a_1 s^2 + a_2 s + a_3} \frac{K_p s + K_i}{s}}{1 + \frac{b}{s^3 + a_1 s^2 + a_2 s + a_3} \frac{K_p s + K_i}{s}} = \frac{b\left(K_p s + K_i\right)}{\left(s^3 + a_1 s^2 + a_2 s + a_3\right)s + b\left(K_p s + K_i\right)}$$
$$= \frac{b\left(K_p s + K_i\right)}{s^4 + a_1 s^3 + a_2 s^2 + \left(a_3 + bK_p\right)s + bK_i} \quad 3.5$$

The closed-loop characteristic equation is

$$\Delta(s) = s^4 + a_1 s^3 + a_2 s^2 + \left(a_3 + bK_P\right)s + bK_i = 0 \quad 3.6$$

If the root loci cross the imaginary axis $s = j\omega$ of the $s = \sigma + j\omega$ plane, then the following is true.

$$
\begin{aligned}
\Delta(j\omega) &= (j\omega)^4 + a_1(j\omega)^3 + a_2(j\omega)^2 + \left(a_3 + bK_p\right)(j\omega) + bK_i \\
&= \omega^4 - a_1 j\omega^3 - a_2\omega^2 + \left(a_3 + bK_p\right)(j\omega) + bK_i \\
&= \underbrace{\left(\omega^4 - a_2\omega^2 + bK_i\right)}_{0} + j\underbrace{\left(-a_1\omega^3 + \left(a_3 + bK_p\right)\omega\right)}_{0} \\
&= 0
\end{aligned}
$$

that is the crossings happen when proportional and integral gains are given by

$$
\begin{aligned}
K_i &= \frac{-\left(\omega^4 - a_2\omega^2\right)}{b} \\
K_P &= \frac{-\left(-a_1\omega^3 + a_3\omega\right)}{b\omega}
\end{aligned}
\qquad 3.7
$$

3.2.1 Illustration of Kharitonov Stability Region

Kharitonov stability criterion states that any K_P and K_i values in the following range guarantees that system in eq 3.5 will be stable. The following example illustrate the Kharitonov stability criterion using the root locus plot of an example system Let us consider a system with poles located at -1,-2 and -4 on an S-plane with transfer function gain of 80.

$$
G_1(s) = \frac{80}{(s+1)(s+2)(s+4)} = \frac{80}{s^3 + 7s^2 + 14s + 8} \qquad 3.8
$$

The zero of the PI compensator of eq 3.4 is located at - Z_c . For example, if we choose the zero location to be at -0.5, then

$$
\begin{aligned}
Z_{c1} &= \frac{K_i}{K_p} = 0.5 \ , \\
K_i &= K_p * Z_{c1} = K_p * 0.5 \ , \\
C_1(s) &= \frac{K_p(s+0.5)}{s}
\end{aligned}
\qquad 3.9
$$

A range of root locus plots for the $\Delta(s)$ in eq 3.6 with the controller numerator (zero term) set to $Z_c = \dfrac{K_i}{K_p} = -0.5, 0, 0.5,\ 1.5,\ 2.5\ \&\ 3.5$ is shown below

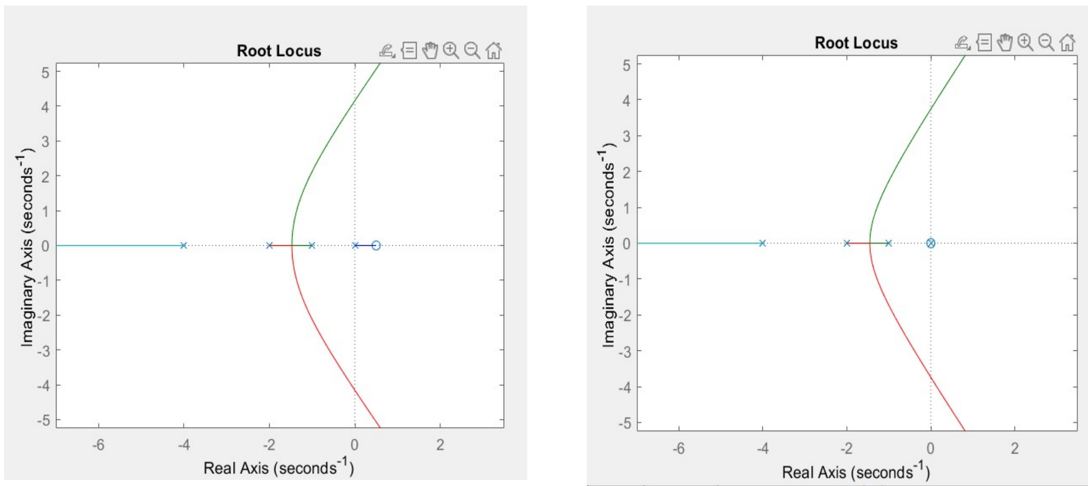

(a) (b)

Figure 3.4: Root Locus of the system with PI controller. (a) Zc = -0.5 (b) Zc = 0

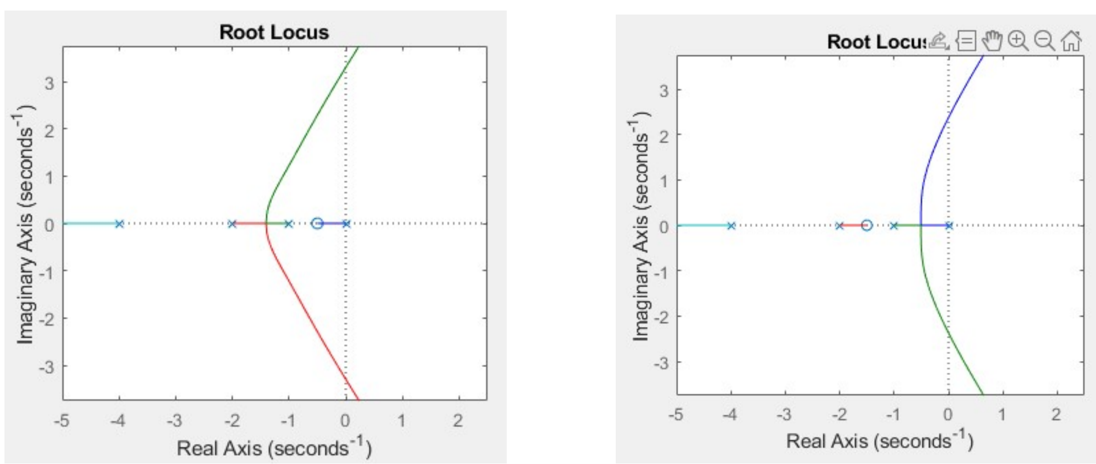

(a) (b)

Figure 3.5: Root Locus of the system with PI controller. (a) Zc = 0.5, (b) Zc = 1.5

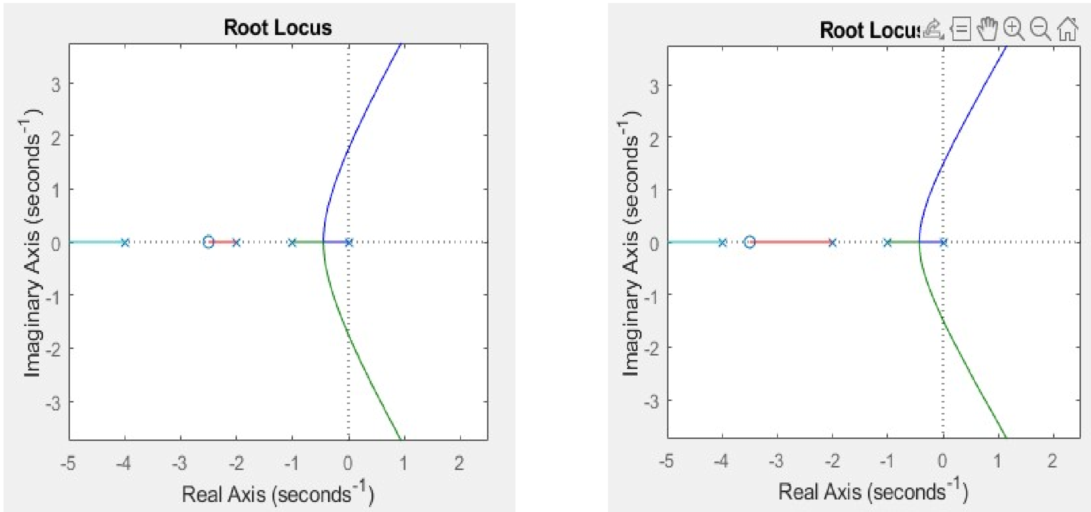

(a) (b)

Figure 3.6: Root Locus of the system with PI controller. (a) Zc = 2.5, (b) Zc = 3.5

When root loci of the system cross imaginary axis then the system transitions from stable state to unstable state. By observing Fig 3.4, 3.5 and 3.6, it is evident that as the location of zero changes in the compensator the frequency(ω) or the location where stable to unstable state transition also changes. Table 3.2 gives cross-over frequency for different zeros locations of compensator.

From eq 3.7 K_p and K_i are given by

$$K_i = \frac{-\left(\omega^4 - 14\omega^2\right)}{80}$$
$$K_P = \frac{-\left(-7\omega^3 + 8\omega\right)}{80\omega} \qquad 3.10$$

To extend the root loci, for determining the stability region of a given system with PI controller for different gain values. A plot is drawn between K_p and K_i varying omega. For all the positive values of gains under the plot the system is stable.

In Fig 3.7 omega (ω) varies from 0 to 4.5 to find gain values (using eq 3.10). The plot between controller gains (K_p and K_i) is as below Fig 3.7. For all the positive values of K_p and K_i under the blue curve the system is stable.

Table 3.2: Root Loci imaginary axis crossover based on Zero location in compensator

$Z_c = \frac{K_i}{K_p}$	**Imaginary axis crossover (ω) from Root Locus**	$K_i = \frac{-\left(\omega^4 - 14\omega^2\right)}{80}$	$K_P = \frac{-\left(-7\omega^3 + 8\omega\right)}{80\omega}$
-0.5	4.1706,-4.1706	1.422	-0.737
0	3.752,-3.752	1.1318	-0.0136
0.5	3.2964,-3.2964	0.4257	0.8508
1	2.8404, -2.8404	0.5982	0.6059
1.5	2.3994,-2.3994	0.5932	0.4037
2	1.9369,-1.9369	0.4806	0.2283
2.5	1.7365,-1.7365	0.4140	0.1639

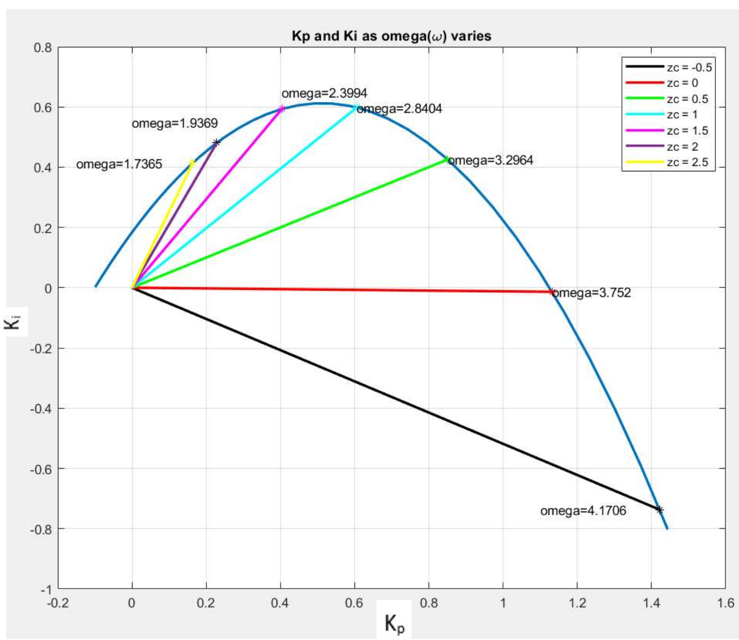

Figure 3.7: Stable values for Kp and Ki from the root-locus plots as omega (ω) vary from 0 to 3.752, illustrating the Kharitonov stability criterion.

As omega values beyond from 3.752 K_i is negative, if K_i is negative zero of the closed-loop transfer functions shifts to positive side of S-plane. If a zero is on the right-hand side of the S-plane and there is a pole at the origin, increasing the controller gains further destabilizes the system.

3.3 Kharitonov Stability Analysis

According to Kharitonov's theorem an interval transfer function is stable if and only if all the terminal Kharitonov plants are stable [9],[19]. C(s) be controller transfer function and if $G(s)$ is an interval plant system in Fig 3.3.

$$G_I(s) = \frac{N(s)}{D(s)} = \frac{q_m s^m + q_{m-1} s^{m-1} + \ldots + q_0}{p_m s^m + p_{m-1} s^{m-1} + \ldots + p_0} \qquad 3.11$$

$N(s)$ is the numerator and $D(s)$ is the denominator.

where $q_i \in [\,\underline{q}_i, \bar{q}_i,]$, i= 0, 1, ..m and pi $\in [\,\underline{p}_i, \bar{p}_i,]$, i= 0, 1, ..n and the Kharitonov polynomials associated with $N(s)$ and $D(s)$ be respectively:

$$\begin{aligned}
N_1(s) &= \underline{q}_0 + \underline{q}_1 s + \overline{q}_2 s^2 + \overline{q}_3 s^3 + \underline{q}_4 s^4 + \underline{q}_5 s^5 + \overline{q}_6 s^6 + \overline{q}_7 s^7 \ldots \\
N_2(s) &= \underline{q}_0 + \overline{q}_1 s + \overline{q}_2 s^2 + \underline{q}_3 s^3 + \underline{q}_4 s^4 + \overline{q}_5 s^5 + \overline{q}_6 s^6 + \underline{q}_7 s^7 \ldots \\
N_3(s) &= \overline{q}_0 + \underline{q}_1 s + \underline{q}_2 s^2 + \overline{q}_3 s^3 + \overline{q}_4 s^4 + \underline{q}_5 s^5 + \underline{q}_6 s^6 + \overline{q}_7 s^7 \ldots \\
N_4(s) &= \overline{q}_0 + \overline{q}_1 s + \underline{q}_2 s^2 + \underline{q}_3 s^3 + \overline{q}_4 s^4 + \overline{q}_5 s^5 + \underline{q}_6 s^6 + \underline{q}_7 s^7 \ldots \\
&\textit{and} \qquad\qquad\qquad\qquad\qquad\qquad\qquad 3.12 \\
D_1(s) &= \underline{p}_0 + \underline{p}_1 s + \overline{p}_2 s^2 + \overline{p}_3 s^3 + \underline{p}_4 s^4 + \underline{p}_5 s^5 + \overline{p}_6 s^6 + \overline{p}_7 s^7 \ldots \\
D_2(s) &= \underline{p}_0 + \overline{p}_1 s + \overline{p}_2 s^2 + \underline{p}_3 s^3 + \underline{p}_4 s^4 + \overline{p}_5 s^5 + \overline{p}_6 s^6 + \underline{p}_7 s^7 \ldots \\
D_3(s) &= \overline{p}_0 + \underline{p}_1 s + \underline{p}_2 s^2 + \overline{p}_3 s^3 + \overline{p}_4 s^4 + \underline{p}_5 s^5 + \underline{p}_6 s^6 + \overline{p}_7 s^7 \ldots \\
D_4(s) &= \overline{p}_0 + \overline{p}_1 s + \underline{p}_2 s^2 + p_3 s^3 + \overline{p}_4 s^4 + \overline{p}_5 s^5 + \underline{p}_6 s^6 + p_7 s^7 \ldots
\end{aligned}$$

By taking all the combinations of the $N_i(s)$ and $D_j(s)$ for i, j = 1,2,3,4, the following sixteen Kharitonov plants can be obtained[9]. $G_{i\,j}(s)$ gives Kharitonov's terminal transfer functions for the interval system determined in $G(s)$ eq 3.11.

$$G_{i\,j}(s) = \frac{N_i(s)}{D_j(s)} \text{ where } i,j = 1,2,3,4 \qquad 3.13$$

As explained in the previous section each transfer function has a stable region which can be determined by varying omega and finding gain values. According to Kharitonov stability of interval transfer function $G(s)$ is intersection of all the stability regions of each transfer functions $G_{i\,j}(s)$. Let a single set of $S(G(s)C(s))$ represent all the values of the parameters of the controller C(s) that stabilize G(s). Then the set of all the stabilizing values of the parameters of a controller that stabilize the interval plant can be written as [9].

$$\begin{aligned} S(G(s)C(s)) &= \bigcap\nolimits_{i,j=1,2,3,4} S(G_{ij}(s)C(s)) \\ &= S(G_{1,1}(s)C(s)) \cap S(G_{1,2}(s)C(s)) \cap \quad \ldots \quad \cap S(G_{4,4}(s)C(s)) \end{aligned} \qquad 3.14$$

3.3.1 Kharitonov Stability with PI Controller

To generalize the control scheme explained in section 3.2 and extend it to interval systems with PI controller. Separating odd and even parts of plant transfer function G(s) by substituting s = jω gives,

$$G(j\omega) = \frac{N_e(-\omega^2) + j\omega N_o(-\omega^2)}{D_e(-\omega^2) + j\omega D_o(-\omega^2)}$$

PI controller transfer function

$$C(s) = \frac{K_p s + K_i}{s}$$

Closed loop characteristic equation of the above unity feedback system in Fig 3.3

$$
\begin{aligned}
1+G(j\omega)C(j\omega) = {} & [K_i N_e(-\omega^2) - K_P\omega^2 N_o(-\omega^2) - \omega^2 D_o(-\omega^2)] \\
& + j\omega[K_p N_e(-\omega^2) + K_i N_o(-\omega^2) + D_e(-\omega^2)]
\end{aligned}
$$

Equating real and imaginary terms in above equation to zero

$$
\begin{aligned}
K_P &= \frac{\omega^2 D_o(-\omega^2)\omega N_o(-\omega^2) - \left[-\omega D_e(-\omega^2) N_e(-\omega^2)\right]}{-\omega^2 N_o(-\omega^2)\omega N_o(-\omega^2) - N_e(-\omega^2)\omega N_e(-\omega^2)} \\
K_i &= \frac{\left[-\omega D_e(-\omega^2)\right]\left[-\omega^2 N_o(-\omega^2)\right] - \omega^2 D_o(-\omega^2)\omega N_e(-\omega^2)}{-\omega^2 N_o(-\omega^2)\omega N_o(-\omega^2) - N_e(-\omega^2)\omega N_e(-\omega^2)}
\end{aligned}
\qquad 3.15
$$

Simplifying above terms gives the following

$$
\begin{gathered}
K_P = \frac{X(\omega)U(\omega) - Y(\omega)R(\omega)}{Q(\omega)U(\omega) - R(\omega)S(\omega)} \\
K_i = \frac{Y(\omega)Q(\omega) - X(\omega)S(\omega)}{Q(\omega)U(\omega) - R(\omega)S(\omega)} \\
Q(\omega) = -\omega^2 N_o(-\omega^2), R(\omega) = N_e(-\omega^2) \\
S(\omega) = \omega N_e(-\omega^2), U(\omega) = \omega N_o(-\omega^2) \\
X(\omega) = \omega^2 D_o(-\omega^2), Y(\omega) = -\omega D_e(-\omega^2)
\end{gathered}
$$

3.3.2 Stability Region of SEDCM with PI Controller

Interval plant in the last row third column of Table 3.1 is considered to find stability region of SEDCM with optimization, apply Kharitonov's stability [5]-[6] condition (eq 3.14) and the method described to find K_P and K_i in (eq 3.15)[5].

$$
\begin{array}{lcl}
q_0 = [3048, 2945] & \textit{and} & p_0 = [90, 86.6] \\
q_1 = [114, -26.27] & & p_1 = [95, 94.6] \;\&\; p_2 = [1,1] \\
N_1(s) = 3048 + 114s & & D_1(s) = 90 + 95s + s^2 \\
N_2(s) = 3048 - 26.27s & & D_2(s) = 90 + 94.6s + s^2 \\
N_3(s) = 2945 + 114s & \textit{and} & D_3(s) = 86.6 + 95s + s^2 \\
N_4(s) = 2945 - 26.27s & & D_4(s) = 86.6 + 94.6s + s^2
\end{array}
$$

Out of sixteen plants derived from the four numerator and four denominator polynomials above (based on eq 3.13) G11, G12, G13, G14, G31, G32, G33 and G34 are stable because the poles and zeros lie on left hand side of S-plane, In order to find the stability region of the remaining transfer functions based on Kharitonov's stability [5].

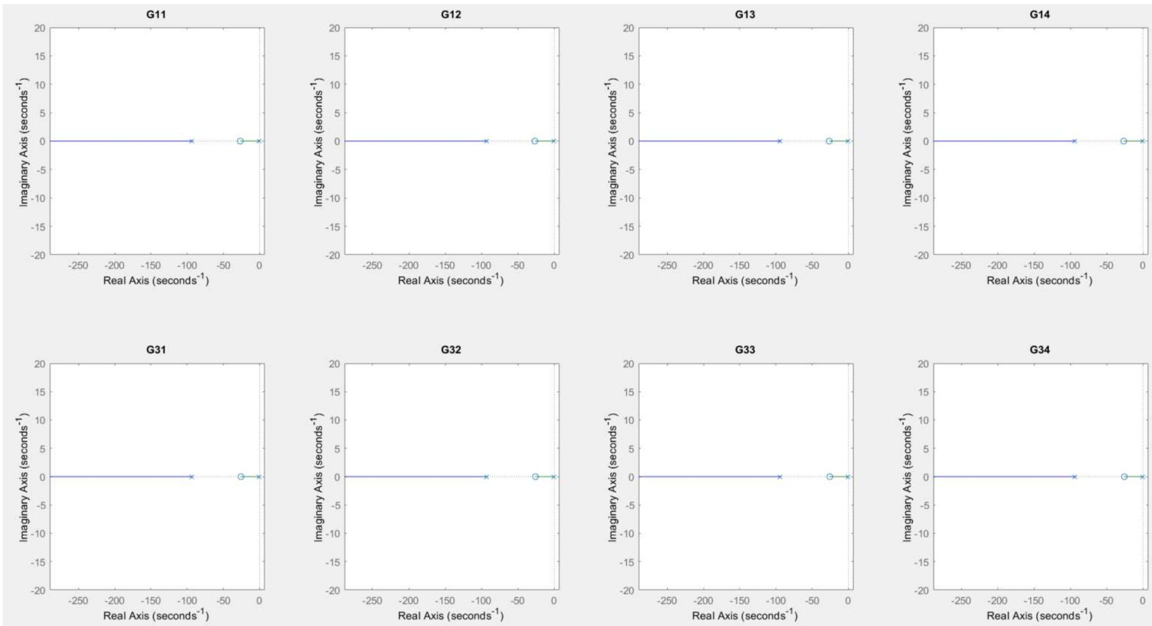

Figure 3.8: Root Locus of $1+K_pG_{ij}(s)=0$ showing stable closed loop characteristic

The root locus analysis shows that G11, G12, G13, G14, G31, G32, G33 and G34 these do not cross the jω - axis. Hence, they don't appear in the Kharitonov analysis. The intersection of stability regions of remaining transfer functions G_{21}, G_{22}, G_{23}, G_{24}, G_{41}, G_{42}, G_{43} and G_{44}.

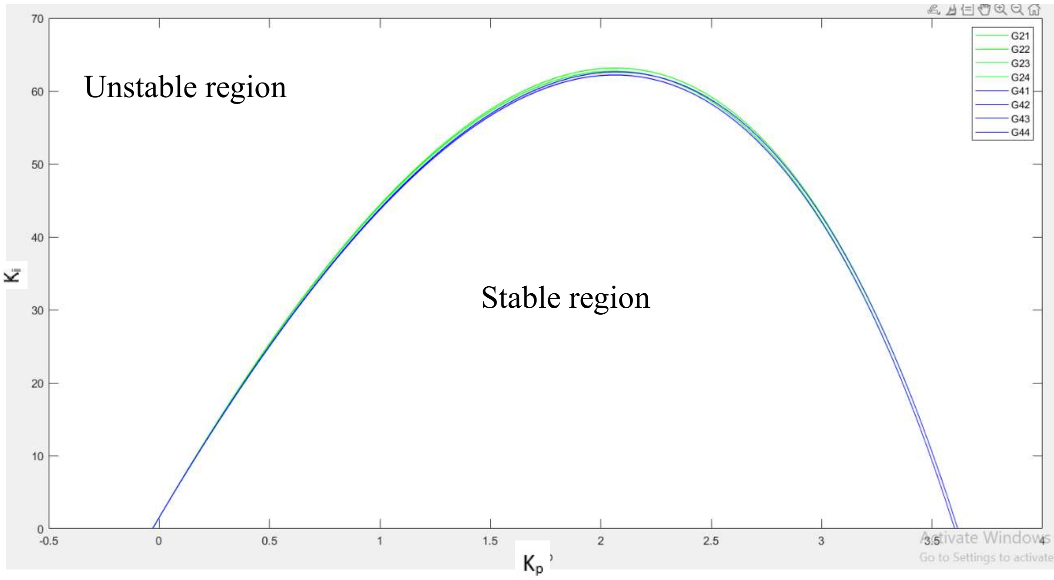

Figure 3.9: Stability region of SEDCM with Optimization algorithm.

3.3.3 Kharitonov Stability with PID Controller

To generalize the control scheme explained in section 3.2 and extending it to interval systems with PID controller. Separating odd and even parts of G(s) by substituting s = jω gives,

$$G(j\omega) = \frac{N_e(-\omega^2) + j\omega N_o(-\omega^2)}{D_e(-\omega^2) + j\omega D_o(-\omega^2)}$$

PID controller transfer function

$$C(s) = K_p + \frac{K_i}{s} + K_d s = \frac{K_d s^2 + K_p s + K_i}{s}$$

Closed loop characteristic equation of the above unity feedback system in Fig8 is

$$\begin{aligned} 1 + G(j\omega)C(j\omega) = {} & [K_i N_e(-\omega^2) - K_p \omega^2 N_o(-\omega^2) - \omega^2 D_o(-\omega^2) - \omega^2 N_e(-\omega^2) K_d] \\ & + j\omega[K_p N_e(-\omega^2) + K_i N_o(-\omega^2) + D_e(-\omega^2) - N_o(-\omega^2) K_d \omega^2] \end{aligned}$$

Equating real and imaginary terms in above equation to zero

$$K_P = \frac{-(\omega^2 N_o(-\omega^2)D_o(-\omega^2) + N_e(-\omega^2)D_e(-\omega^2))}{\omega^2 N_o^{\,2}(-\omega^2) + N_e^{\,2}(-\omega^2)}$$

$$K_i = \frac{\omega^2 N_e(-\omega^2)D_o(-\omega^2) - \omega^2 N_o(-\omega^2)D_e(-\omega^2) + K_d(\omega^2 N_e^{\,2}(-\omega^2) + \omega^4 N_0^{\,2}(-\omega^2))}{\omega^2 N_o^{\,2}(-\omega^2) + N_e^{\,2}(-\omega^2)}$$

If $K_d = 0$ then PID equations for gains will be equivalent to PI equations of gains eq 3.12. Further studies can be pursued by setting K_d to various values.

Fig 3.9 shows the stable region for picking K_i and K_p values for the optimum SEDCM interval model. The equations for determining the K_p,K_i, and K_d values for different omega values are given in section 3.3.3.

CHAPTER FOUR

DLAC CONTROLLER DESIGN AND IMPLEMENTATION

To control the speed of the motor, it is necessary to design a controller for the motor with an optimization algorithm. Recognizing that an SEDC motor with voltage optimization functions as a non-linear system, the Direct Lyapunov Adaptive Controller (DLAC) technique, an extension of the Lyapunov Stability Criterion (LSC), is employed for the design of an adaptive controller. This approach guarantees stability but ensures effective speed regulation, a critical aspect of motor performance. In DLAC controller parameters are updated/adapted based on the error, and a derivative of error is chosen to be an exponential function to vanish at an exponential rate[4].

A DLAC scheme for controlling the speed of an optimized SEDC motor, shown in Fig 4.1, can be represented as a DCLA with an uncertain interval system, shown in Fig 4.2. We present a direct application of LSC to the latter system.

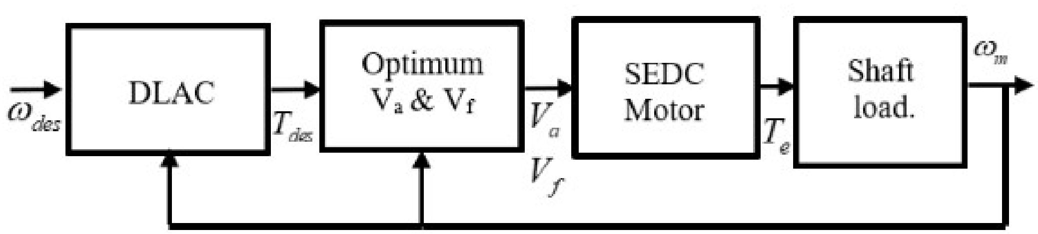

Figure 4.1: Optimized SEDCM with the DLAC

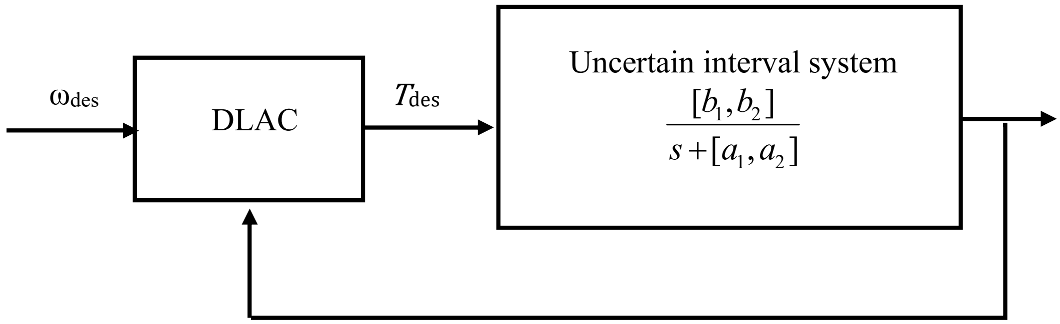

Figure 4.2: Optimized SEDCM as an uncertain interval system

4.1 Lyapunov Stability Criterion

The Lyapunov Stability Criterion (LSC) considers a system described by an n-th order homogeneous nonlinear vector differential equation given by

$$\frac{d\mathbf{x}}{dt} = \mathbf{f}(\mathbf{x}) \qquad\qquad \mathbf{x} \in \Re^n$$

with $\mathbf{x} = \mathbf{x}_0 = \mathbf{0}$ as a singular (equilibrium) point, where

$$\left.\frac{d\mathbf{x}}{dt}\right|_{\mathbf{x}=\mathbf{x}_0=0} = \mathbf{f}(0) = 0$$

The LSC states that the singular point is asymptotically stable if a positive measure of $\mathbf{x}$ represented by

$$\mathrm{V}(\mathrm{x}(\mathrm{t})) > 0, \quad \forall \ \ \mathrm{x} \neq 0$$

can be found such that its time derivative is negative

$$\frac{d\mathrm{V}(x(\mathrm{t}))}{dt} < 0, \forall x$$

4.2 DLAC Controller Design

4.2.1 Tracking and Parameter Estimation Errors

The DLAC scheme for the uncertain interval system in Fig 4.2 can be re-expressed as in Fig 4.1, where parameters $a, b \,\&\, c$ are the unknowns. Note that c is added here to represent an unknown constant, for completeness.

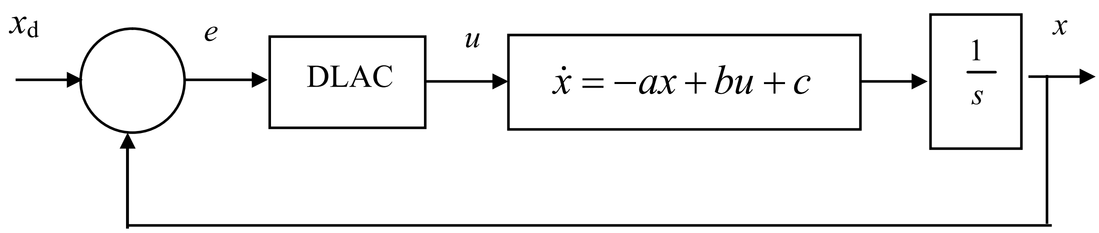

Figure 4.3: First order linear plant model with controller

The plant

$$\dot{x} = -ax + bu + c \tag{4.1}$$

produces the state x. The goal is to find a tracking control u such that x will track x_d (desired speed) and to set the tracking error.

$$e = x_d - x \tag{4.2}$$

such that the dynamical behavior of the error follows the

$$\dot{e} = -ke, \quad k > 0 \tag{4.3}$$

where $k > 0$. That is, the error will vanish at an exponential rate as in

$$e(t) = e_0 \exp(-kt) \quad as \quad t \to \infty \quad e(t) \to 0$$

The error rate is given by

$$\dot{e} = \dot{x}_d - \dot{x} = \dot{x}_d - (-ax + bu + c) \tag{4.4}$$

Because parameters a, b & c are unknown, we substitute their estimates

$\hat{a}, \hat{b}$ & $\hat{c}$, with $\hat{b} > 0$ in the controller.

$$u = \frac{1}{\hat{b}}\left(k\,e + \dot{x}_d - (-\hat{a}x + \hat{c})\right) \qquad 4.5$$

substituting 4.5 in 4.3 to obtain the tracking behavior.

$$\begin{aligned} \dot{e} &= \dot{x}_d - (-ax + b\frac{1}{\hat{b}}\left(k\,e + \left(\dot{x}_d - (-\hat{a}x + \hat{c})\right)\right) + c) \\ &= -\frac{b}{\hat{b}}k\ e + \tilde{a}x - \tilde{c} - \frac{\tilde{b}}{\hat{b}}\left(\dot{x}_d - (-\hat{a}x + \hat{c})\right) \end{aligned} \qquad 4.6$$

where $\tilde{a} = a - \hat{a},\ \tilde{b} = b - \hat{b}$ & $\tilde{c} = c - \hat{c}$ are unknown errors in the parameter estimation.

Need to estimate $\hat{a},\ \hat{b}$ & $\hat{c}$ such that $\tilde{a} \to 0,\ \tilde{b} \to 0$ & $\tilde{c} \to 0$ as $t \to \infty$.

4.2.2 Lyapunov Function

Consider the Lyapunov candidate that comprises the estimation errors.

$$V = \frac{1}{2}e^2 + \frac{1}{2}q_1\tilde{a}^2 + \frac{1}{2}q_2\tilde{b}^2 + \frac{1}{2}q_3\tilde{c}^2 \qquad 4.7$$

and derive its derivative with the help of 4.6

$$\begin{aligned} \dot{V} &= e\dot{e} + q_1\tilde{a}\dot{\tilde{a}} + q_2\tilde{b}\dot{\tilde{b}} + q_3\tilde{c}\dot{\tilde{c}} \\ &= e\left(-\frac{b}{\hat{b}}k\,e + \tilde{a}x - \tilde{c} - \frac{\tilde{b}}{\hat{b}}\left(\dot{x}_d - (-\hat{a}x + \hat{c})\right)\right) + q_1\tilde{a}\dot{\tilde{a}} + q_2\tilde{b}\dot{\tilde{b}} + q_3\tilde{c}\dot{\tilde{c}} \\ &= -\frac{b}{\hat{b}}k\,e^2 + \tilde{b}\underbrace{\left(q_2\dot{\tilde{b}} - \frac{e}{\hat{b}}\left(\dot{x}_d - (-\hat{a}x + \hat{c})\right)\right)}_{set\,to\,0} + \tilde{a}\underbrace{\left(q_1\dot{\tilde{a}} + ex\right)}_{set\,to\,0} + \tilde{c}\underbrace{\left(q_3\dot{\tilde{c}} - e\right)}_{set\,to\,0} \end{aligned} \qquad 4.8$$

From inspection, if

$$\dot{\tilde{a}} = -\frac{1}{q_1}ex$$
$$\dot{\tilde{b}} = \frac{1}{q_2}\frac{e}{\hat{b}}\left(\dot{x}_d - (-\hat{a}x + \hat{c})\right) \qquad 4.9$$
$$\dot{\tilde{c}} = \frac{1}{q_3}e$$

then

$$\dot{V} = -\frac{b}{\hat{b}}ke^2 \qquad 4.10$$

4.2.3 Closed Loop DLAC System.

The dynamics of the concerned variables can be collectively represented as

$$\begin{bmatrix} \dot{e} \\ \dot{\tilde{a}} \\ \dot{\tilde{b}} \\ \dot{\tilde{c}} \end{bmatrix} = \begin{bmatrix} -\frac{b}{\hat{b}}k & x & -\frac{1}{\hat{b}}\left(\dot{x}_d - (-\hat{a}x + \hat{c})\right) & -1 \\ -\frac{1}{q_1}x & 0 & 0 & 0 \\ \frac{1}{q_2}\frac{1}{\hat{b}}\left(\dot{x}_d - (-\hat{a}x + \hat{c})\right) & 0 & 0 & 0 \\ \frac{1}{q_3} & 0 & 0 & 0 \end{bmatrix} \begin{bmatrix} e \\ \tilde{a} \\ \tilde{b} \\ \tilde{c} \end{bmatrix} \qquad 4.11$$

The Lyapunov function is given by.

$$\begin{aligned} V &= \frac{1}{2}e^2 + \frac{1}{2}q_1\tilde{a}^2 + \frac{1}{2}q_2\tilde{b}^2 + \frac{1}{2}q_3\tilde{c}^2 \; > \; 0 \\ \dot{V} &= -\frac{b}{\hat{b}}ke^2 \; < \; 0 \end{aligned} \qquad 4.12$$

Therefore the

$$\begin{bmatrix} e \\ \tilde{a} \\ \tilde{b} \\ \tilde{c} \end{bmatrix} \to \begin{bmatrix} 0 \\ 0 \\ 0 \\ 0 \end{bmatrix} \quad as \;\; t \to \infty \qquad 4.13$$

4.2.4 Near Steady-State Condition

To arrive at the update expressions for the parameter estimates $\hat{a}$, $\hat{b}$ & $\hat{c}$, we will consider when the unknown parameters is near their steady-state condition, i.e., $\dot{a} \approx 0$, $\dot{b} \approx 0$ & $\dot{c} \approx 0$.

Hence, we set $\dot{\tilde{a}} = -\dot{\hat{a}}$, $\dot{\tilde{b}} = -\dot{\hat{b}}$ & $\dot{\tilde{c}} = -\dot{\hat{c}}$, and the update for the parameters follows as

$$\begin{aligned} \dot{\hat{a}} &= \frac{1}{q_1} e x \\ \dot{\hat{b}} &= -\frac{1}{q_2}\frac{e}{\hat{b}}\left(\dot{x}_d - (-\hat{a}x + \hat{c})\right) \\ \dot{\hat{c}} &= -\frac{1}{q_3} e \end{aligned} \qquad 4.14$$

The Direct Lyapunov-based Adaptive Control (DLAC) is thus given by

$$u = \frac{1}{\hat{b}}\left(k\,e + \dot{x}_d - (-\hat{a}x + \hat{c})\right) \qquad 4.15$$

4.2.5 Implementation of DLAC Algorithm

Validation of the proposed concept made using Matlab Simulink, demonstrating the effectiveness and feasibility of the proposed differentiation-based minimization technique and the adaptive controller in achieving stable and regulated motor speed

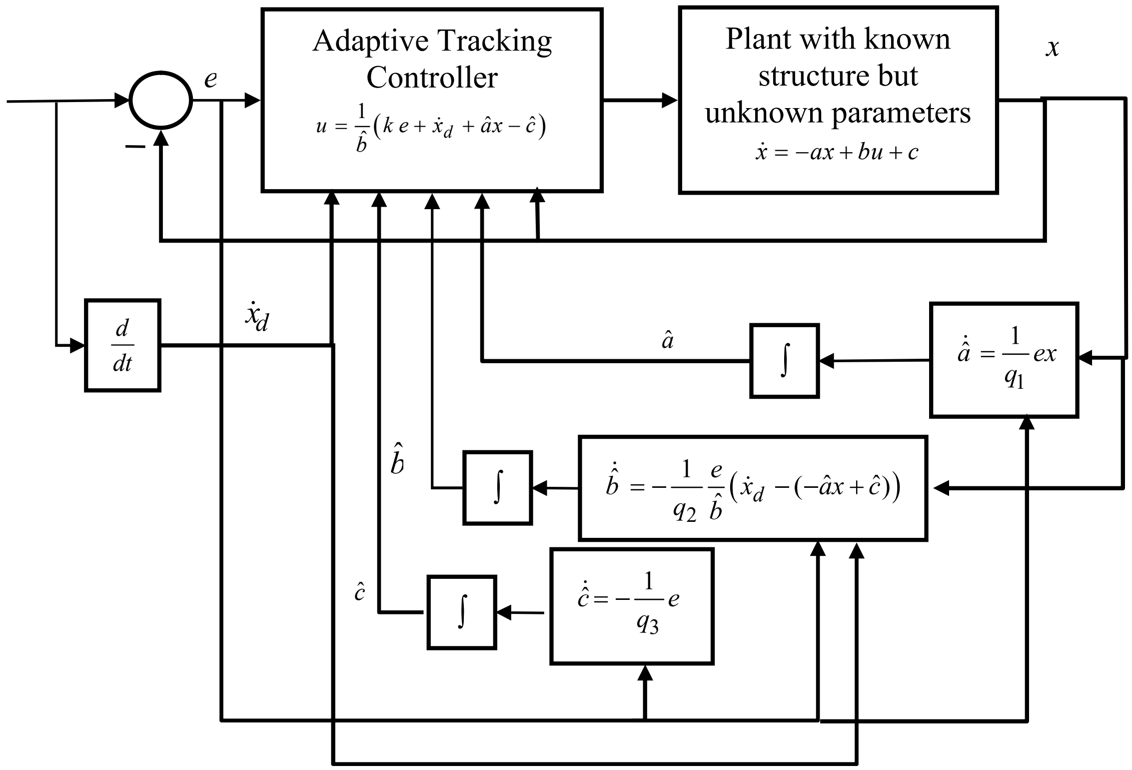

Figure 4.4: Block diagram for Matlab implementation for DLAC

Need to specify desired convergence rate k and weights for Lyapunov function q_1, q_2 & q_3.

4.3 Implementation of DLAC for SEDCM with Optimization

To control the non-linear system of SEDCM with optimization DLAC design technique is proposed to ensure both stability and reach desired the speed.

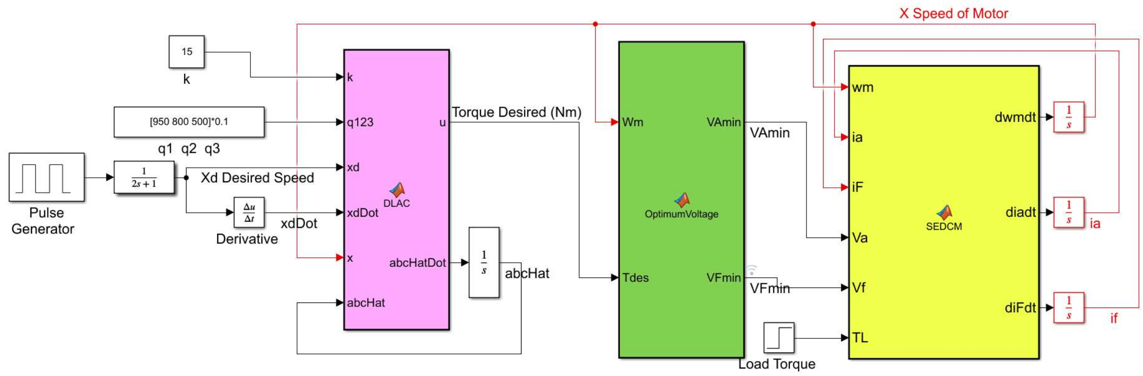

Figure 4.5: Matlab implementation of DLAC with SEDCM with optimization

4.4 Results

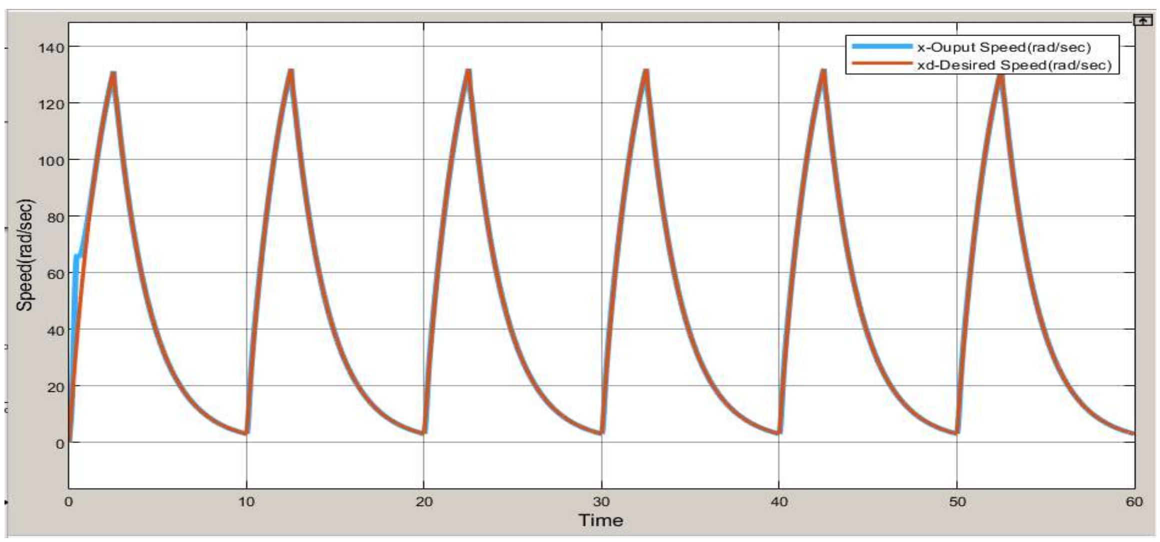

Figure 4.6: Desired speed vs Output speed

The DLAC controller recommended in this chapter proves that non-linearity introduced in the SEDCM because of optimization can be controlled. From Fig 4.7 desired speed can be obtained, Table 4.1 provides the values of variables which need to be tuned based on the desired speed limits, from Fig 4.8 one can observe how the variables are adapting from initial values provided.

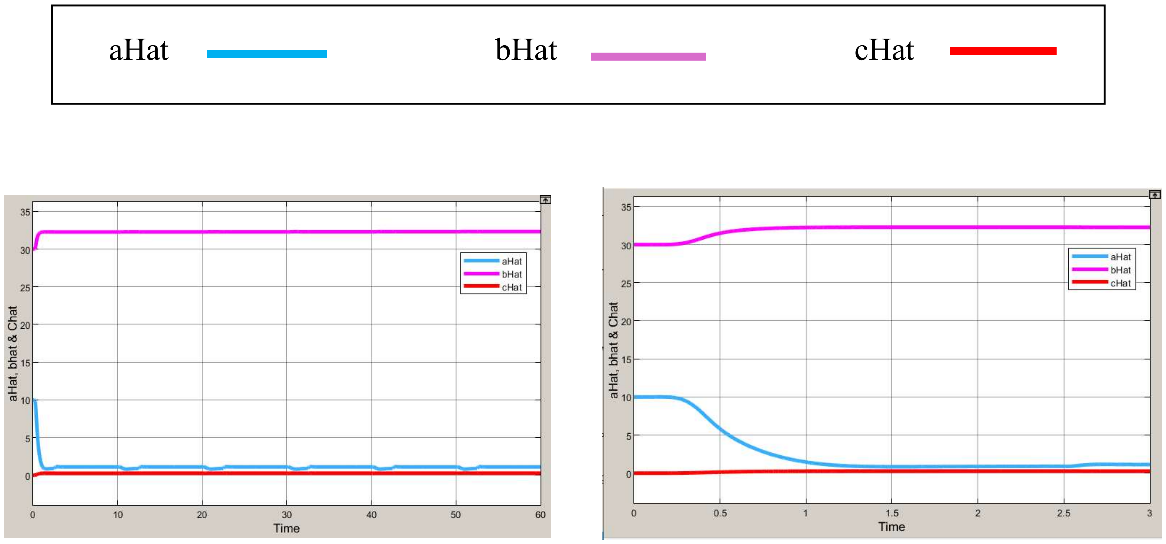

Figure 4.7: aHat, bHat and cHat adaptation

Table 4.1: Speed vs q1,q2 and q3

ω_m (rad/sec)	**q1**	**q2**	**q3**
10	0.95	0.8	0.5
50	8.55	7.2	4.5
100	9.5	8	5
180	95	80	50

CHAPTER FIVE

UNIFIED ROBUST CONTROLLER FOR DC – DC CONVERTERS

According to Fig 2.2 SEDC motor receives direct armature and field voltage inputs. However, in practical applications, the voltages supplied to the motor are regulated through the utilization of a DC-DC converter. Typically, this involves the integration of either a buck converter or a boost converter to control and optimize the voltage levels delivered to the motor in accordance with operational requirements.

To design the Buck or Boost converter, one needs to have knowledge or background about the amount of power consumption, frequency of operation, and peak voltage. In this chapter, an uncertain interval transfer function-based controller design technique is discussed to control the voltage output of DC converters.

5.1 DC-DC Converters as Uncertain Interval Transfer Function

A buck, boost or buck-boost converter can be formulated as an uncertain interval system, i.e.,

$$V_o = Gu \qquad G \in [g_1,\ g_2]$$

where,

$V_o =$ output voltage of the converter
$u = D =$ input duty cycle to the converter
$G =$ uncertain gain value that varies in the interval $[g_1,\ g_2]$

The transfer gain G for each of the converters is shown in Column 3 of Table 5.1.

Column 4 shows that the intervals for the transfer gain G for $u = D \in [0.1, 0.9]$ and

$V_{dc} = 5\text{V}$, that is

$$
\begin{array}{ll}
\text{Boost converter} & G \in [20, 55] \\
\text{Buck converter} & G \in [5, \ \ 5] \\
\text{Buck-boost converter} & G \in [-5.5, \ -50]
\end{array}
$$

Table 5.1: DC-DC transfer functions of converter

Converter	**DC-DC transfer function**	**Output to Duty cycle ratio transfer function**	**Duty cycle vs G**
Boost converter	$\frac{V_0}{V_{dc}} = \frac{1}{(1-D)}$	$G = \frac{V_0}{D} = \frac{V_{dc}}{D(1-D)}$	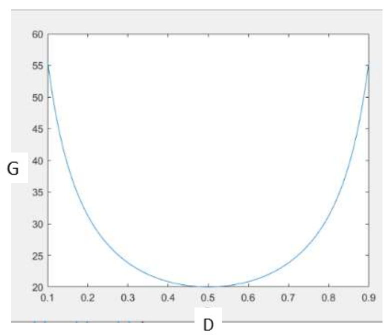
Buck convert	$\frac{V_0}{V_{dc}} = D$	$G = \frac{V_0}{D} = V_{dc}$	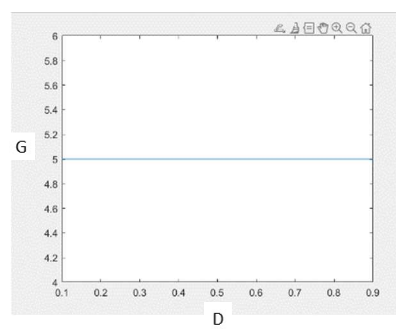

Table 5.1: DC-DC transfer functions of converter-continued

Converter	**DC-DC transfer function**	**Output to Duty cycle ratio transfer function**	**Duty cycle vs G**
Buck-Boost converter	$\frac{V_0}{V_{dc}} = \frac{-D}{(1-D)}$	$G = \frac{V_0}{D} = \frac{V_{dc}}{(1-D)}$	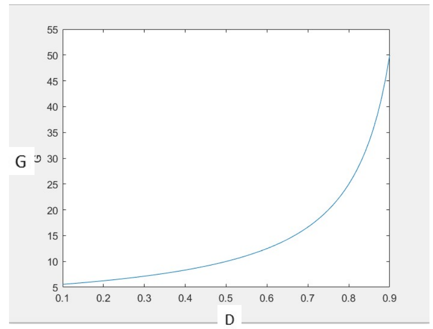

5.2 Design of Unified Robust DC Converter Controller

5.2.1 Unified Robust Controller Design

A PI control scheme for the uncertain DC-DC converter is shown in Fig 5.1.

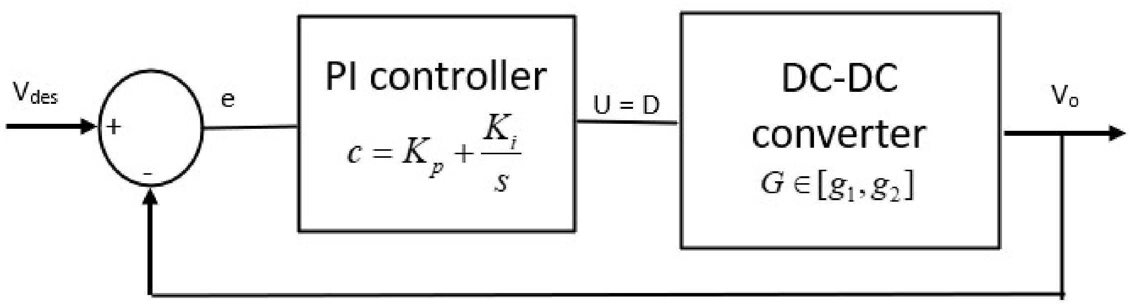

Figure 5.1: Block diagram of DC converter with controller

The unity feedback system with a PI controller C and a plant G. Yields the closed-loop control system

$$\frac{V_o(s)}{V_{des}(s)} = \frac{GC}{1+GC} = \frac{Gk_p(s+\frac{K_i}{k_p})}{s(1+GK_p)+GK_i} = \frac{GK_p(s+z_c)}{(1+GK_p)(s+\frac{GK_i}{1+GK_p})}$$

If $Gk_p >> 1$, then $1+Gk_p \to Gk_p$ and the closed-loop transfer function approaches

$$\lim_{GK_p>>1} \frac{GC}{1+GC} = \lim_{GK_p>>1} \frac{GK_p(s+z_c)}{(1+GK_p)(s+\frac{GK_p}{1+GK_p}z_c)} \to 1$$

The closed-loop transfer function approaches 1 means that the output follows the input almost instantly. The robustness of the closed-loop transfer function is thus achieved by

$$GK_p >> 1$$

Taking $G \in [g_1,\ g_2]$ into account,

$$K_p \ >> \ \frac{1}{G} \ >> \ \frac{1}{\min(g_1,\ g_2)}$$

It follows that

$$K_i \ = z_c \ K_p$$

This last two terms is the gist of the unified robust PI controller for the buck, boost and buck-boost controllers.

The closed-loop PI control DC converter system can be expressed as

$$y(s) = K\frac{s+z_c}{s+Kz_c}r(s)\ , \qquad K = \frac{GK_p}{1+GK_p} \ \in [0,1) \ \text{ as } \ GK_p \in [0,\infty)$$

If $r(s) = \frac{1}{s}$ is a unit step reference, it can be shown using partial fraction expansion that

$$y(s) = \frac{1}{s} + \frac{K-1}{s+K\,z_c}$$

The inverse Laplace transform yields

$$y(t) = 1 + (K-1)\,e^{-Kz_c t}$$

The plot of the unit step responses as K varies is shown in the figure below. It shows that the response y(t) tends to 1 as K approaches 1, implying quickness or near instantaneousness in response. The response analysis demonstrates the effect of pole-zero cancellation, featured in the closed-loop system.

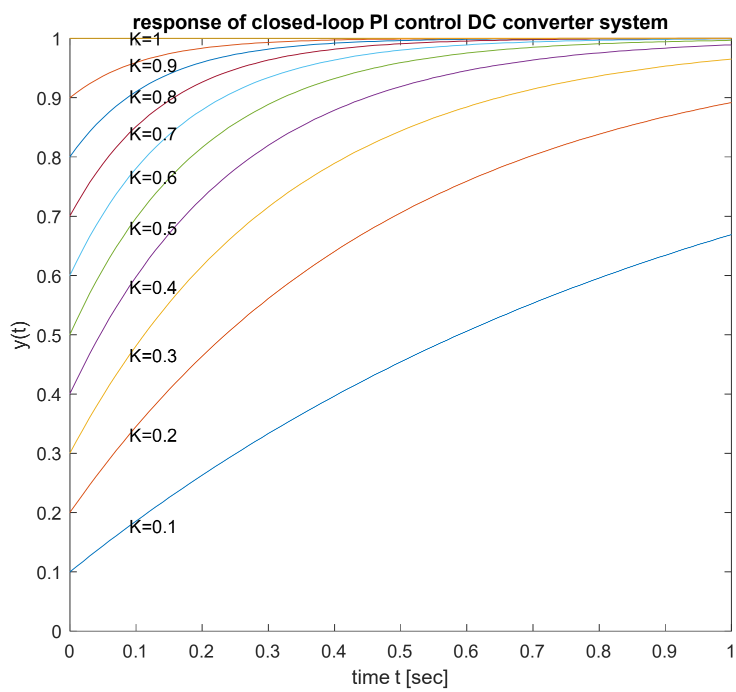

Figure 5.2: Response of CLTF to variable K

5.2.2 Numerical Illustration of the Controller Developed

The tables provided below signify how the values of K_p effects the location of Pole and zero in the closed loop transfer function of DC converters

5.2.3 Boost Converter

Table 5.2: Boost converter closed loop transfer functions when K_p = 5

V_{dc} = 5V		Zero location in PI Controller	$K_P = 5,\ K_i = 50$		Closed-loop transfer function
			Gk_p	$1+Gk_p$	
D = 0.1, 0.9	G = 55.5	$z_c = 10$	277.5	278.5	$\frac{277.5(s+10)}{278.5(s+9.96)}$
D = 0.2, 0.8	G = 31.2	$z_c = 10$	156	157	$\frac{156(s+10)}{157(s+9.93)}$
D = 0.3, 0.7	G = 23.8	$z_c = 10$	119	120	$\frac{119(s+10)}{120(s+9.92)}$
D = 0.4, 0.6	G = 20.8	$z_c = 10$	104	105	$\frac{104(s+10)}{105(s+9.91)}$
D = 0.5	G = 20	$z_c = 10$	100	101	$\frac{100(s+10)}{101(s+9.90)}$

Table 5.3: Boost converter closed loop transfer functions when K_p = 0.5

V_{dc} = 5V		Zero location in PI Controller	$K_P = 0.5,\ K_i = 5$		Closed-loop transfer function
			Gk_p	$1+Gk_p$	
D = 0.1, 0.9	G = 55.5	$z_c = 10$	27.7	28.7	$\frac{27.7(s+10)}{28.7(s+9.65)}$
D = 0.2, 0.8	G = 31.2	$z_c = 10$	15.6	16.6	$\frac{15.6(s+10)}{16.6(s+9.4)}$
D = 0.3, 0.7	G = 23.8	$z_c = 10$	11.9	12.9	$\frac{11.9(s+10)}{12.9(s+9.25)}$
D = 0.4, 0.6	G = 20.8	$z_c = 10$	10.4	11.4	$\frac{10.4(s+10)}{11.4(s+9.12)}$
D = 0.5	G = 20	$z_c = 10$	10	11	$\frac{10(s+10)}{11(s+9.1)}$

Table 5.4: Boost converter closed loop transfer functions when K_p = 0.05

V_{dc} = 5V		Zero location in PI Controller	K_P = 0.05, K_i = .5		Closed-loop transfer function
			Gk_p	$1+Gk_p$	
D = 0.1, 0.9	G = 55.5	$z_c = 10$	2.77	3.77	$\frac{2.77(s+10)}{3.77(s+7.35)}$
D = 0.2, 0.8	G = 31.2	$z_c = 10$	1.56	2.56	$\frac{1.56(s+10)}{2.56(s+6.09)}$
D = 0.3, 0.7	G = 23.8	$z_c = 10$	1.19	2.19	$\frac{1.19(s+10)}{1.29(s+5.43)}$
D = 0.4, 0.6	G = 20.8	$z_c = 10$	1.04	2.04	$\frac{1.04(s+10)}{2.04(s+5.1)}$
D = 0.5	G = 20	$z_c = 10$	1.0	2.0	$\frac{1(s+10)}{2(s+5)}$

Table 5.5: Boost converter interval transfer functions w.r.t K_p .

Location of zero in the PI controller	Interval transfer function
$z_c = 10$, k_p = 5, k_i =50, V_{dc} = 5V	$\frac{[100, 277.5](s+10)}{[101, 278.5](s+[9.90, 9.96])}$
$z_c = 10$, k_p = .5, k_i =5, V_{dc} = 5V	$\frac{[10, 27.75](s+10)}{[11, 27.85](s+[9.1, 9.65])}$
$z_c = 10$, k_p = .05, k_i =5, V_{dc} = 5V	$\frac{[1, 2.77](s+10)}{[2, 3.77](s+[5, 7.35])}$

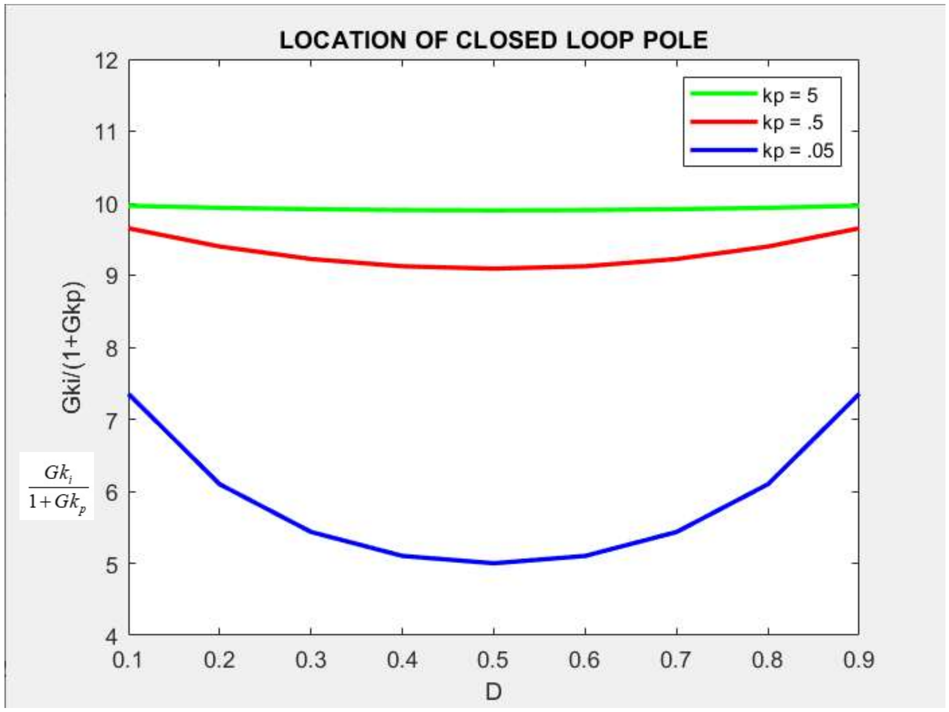

Figure 5.3: Pole location based on value of K_p for Boost converter

5.2.4 Buck Converter

Table 5.6: Buck converter closed loop transfer function when K_p = 5

V_{dc} = 5V		Zero location in PI Controller	$K_P = 5,\ K_i = 50$		Closed-loop transfer function
			Gk_p	$1+Gk_p$	
D = 0.1-0.9	G = 5	$z_C = 10$	25	26	$\frac{25(s+10)}{26(s+9.62)}$

Table 5.7: Buck converter closed loop transfer function when K_p = 0.5

V_{dc} = 5V		Zero location in PI Controller	$K_P = 0.5,\ K_i = 5$		Closed-loop transfer function
			Gk_p	$1+Gk_p$	
D = 0.1-0.9	G = 5	$z_C = 10$	2.5	3.5	$\frac{2.5(s+10)}{3.5(s+7.14)}$

Table 5.8: Buck converter closed loop transfer function when K_p = 0.05

V_{dc} = 5V		Zero location in PI Controller	K_P = 0.05, K_i =0.5		Closed-loop transfer function
			Gk_p	$1+Gk_p$	
D = 0.1- 0.9	G = 5	$z_c = 10$	0.25	1.25	$\frac{0.25(s+10)}{1.25(s+2)}$

Table 5.9: Buck converter interval transfer function w.r.t K_p

Location of zero in the PI controller	Interval transfer function
$z_c = 10$, k_p = 5, k_i=50, V_{dc} = 5V	$\frac{25(s+10)}{26(s+9.62)}$
$z_c = 10$, k_p = .5, k_i=5, V_{dc} = 5V	$\frac{2.5(s+10)}{3.5(s+7.14)}$
$z_c = 10$, k_p = .05, k_i=5, V_{dc} = 5V	$\frac{0.25(s+10)}{1.25(s+2)}$

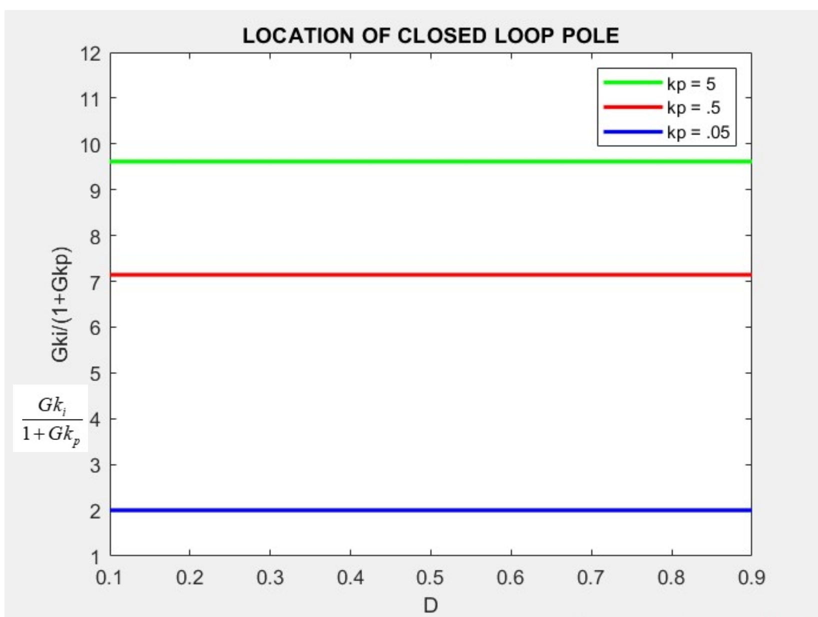

Figure 5.4: Pole location based on value of K_p for Buck converter

5.2.5 Buck-Boost Converter

Table 5.10: Buck-Boost converter closed loop transfer functions when K_p = 5

V_{dc} = 5V		Zero location in PI Controller	$K_p = 5,\ K_i = 50$		Closed-loop transfer function
			Gk_p	$1+Gk_p$	
D = 0.1	G = -5.55	$z_c = 10$	27.78	26.78	$\frac{27.78(s+10)}{26.78(s+9.65)}$
D = 0.3	G = -7.14	$z_c = 10$	35.72	34.71	$\frac{35.72(s+10)}{34.71(s+9.73)}$
D = 0.5	G = -10	$z_c = 10$	50	49	$\frac{50(s+10)}{49(s+9.8)}$
D = 0.7	G = -16.6	$z_c = 10$	83	82	$\frac{83(s+10)}{82(s+9.88)}$
D = 0.9	G = -50	$z_c = 10$	250	249	$\frac{250(s+10)}{249(s+9.6)}$

Table 5.11: Buck-Boost converter closed loop transfer functions when K_p = 0.5

V_{dc} = 5V		Zero location in PI Controller	$K_p = 0.5,\ K_i = 5$		Closed-loop transfer function
			Gk_p	$1+Gk_p$	
D = 0.1	G = -5.55	$z_c = 10$	2.778	1.778	$\frac{2.778(s+10)}{1.778(s+7.35)}$
D = 0.3	G = -7.14	$z_c = 10$	3.572	2.572	$\frac{3.572(s+10)}{2.572(s+7.81)}$
D = 0.5	G = -10	$z_c = 10$	5.0	4.0	$\frac{5(s+10)}{4(s+8.3)}$
D = 0.7	G = -16.6	$z_c = 10$	8.3	7.3	$\frac{8.3(s+10)}{7.3(s+8.92)}$
D = 0.9	G = -50	$z_c = 10$	25.0	24	$\frac{25(s+10)}{24(s+9.61)}$

Table 5.12: Buck-Boost converter closed loop transfer functions when K_p = 0.05

Vdc = 5V		Zero location in PI Controller	K_P = 0.05, K_i = .5		Closed-loop transfer function
			Gk_p	$1+Gk_p$	
D = 0.1	G = -5.55	$z_c = 10$	0.278	0.72	$\frac{0.278(s+10)}{0.72(s+2.17)}$
D = 0.3	G = -7.14	$z_c = 10$	0.36	0.64	$\frac{0.36(s+10)}{0.64(s+2.63)}$
D = 0.5	G = -10	$z_c = 10$	0.5	0.5	$\frac{0.5(s+10)}{0.5(s+3.33)}$
D = 0.7	G = -16.6	$z_c = 10$	0.83	0.17	$\frac{0.83(s+10)}{0.17(s+4.54)}$
D = 0.9	G = -50	$z_c = 10$	2.5	1.5	$\frac{2.5(s+10)}{1.5(s+7.14)}$

Table 5.13: Buck-Boost converter interval transfer function w.r.t K_p

Location of zero in the PI controller	Interval transfer function
$z_c = 10$, K_p = 5, K_i = 50, V_{dc} = 5V	$\frac{[27.78, 250](s+10)}{[26.78, 249](s+[9.65, 9.6])}$
$z_c = 10$, K_p = .5, K_i = 5, V_{dc} = 5V	$\frac{[2.778, 25](s+10)}{[1.778, 24](s+[7.335, 9.61])}$
$z_c = 10$, K_p = .05, K_i = 5, V_{dc} = 5V	$\frac{[0.278, 2.5](s+10)}{[0.72, 3.5](s+[2.17, 7.14])}$

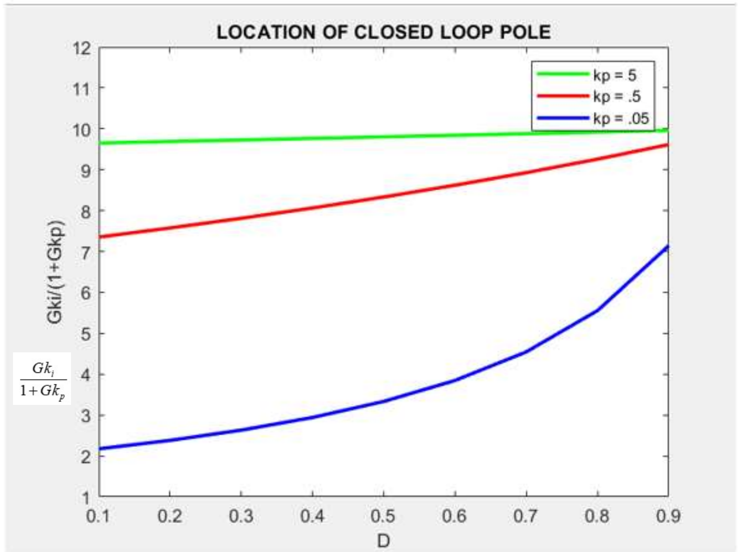

Figure 5.5: Pole location based on value of K_p for Buck-Boost converter

From the data presented in the above tables it is evident that when $GK_p >> 1$ the DC converters closed loop transfer function can be approximated to one. Which implies that output voltage follows the input reference voltage.

5.3 Hardware Component Level Simulations and Results

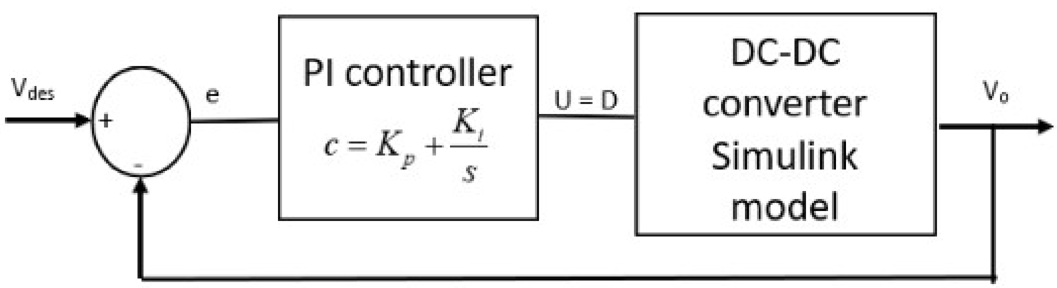

Figure 5.6: Block diagram of DC converter with controller

5.3.1 Boost Converter with PI Controller

A boost converter steps up the input voltage to a higher output voltage. It operates on the principle of energy storage in an inductor and energy transfer to the load through a switch (typically a transistor) and a diode. Boost converter requires precise control and design to avoid instability and oscillations. Implementation of circuits is done using Matlab Simscape. Table 5.14 shows the specification of Boost Converter chosen to design and simulate a PI controller technique discussed above.

Table 5.14: Boost converter parameters

Parameter	**Value**
Input DC Voltage	V_{dc} = 5 Volts
Inductance	L = 2.58 µH
Capacitor	C = 100 µF
Load resistor	R = 56 ohms
Frequency	F = 40000 Hz

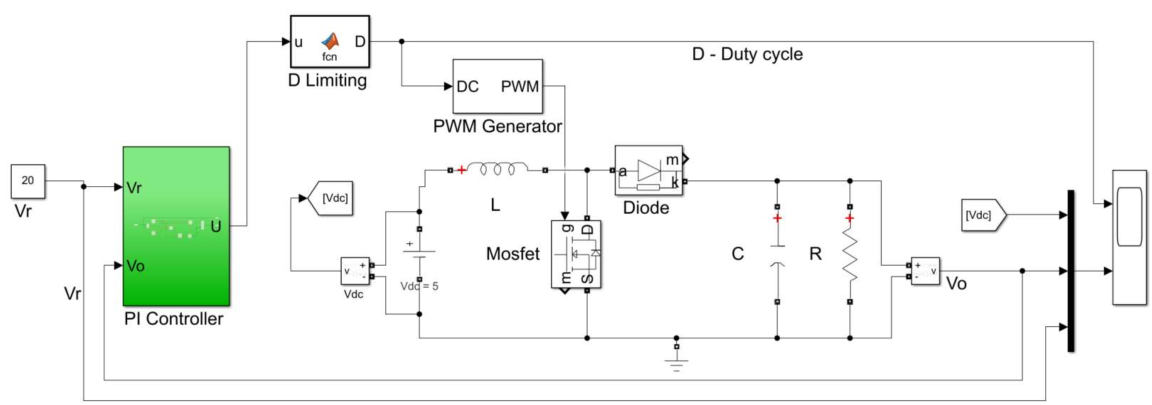

Figure 5.7: Boost converter with controller

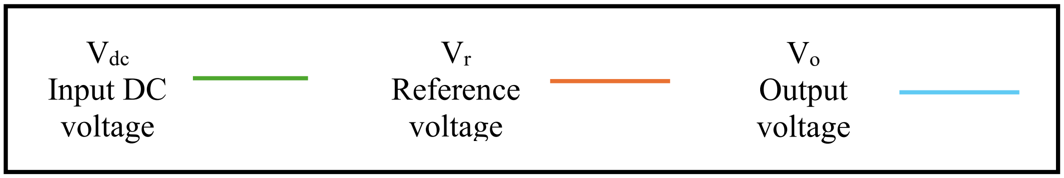

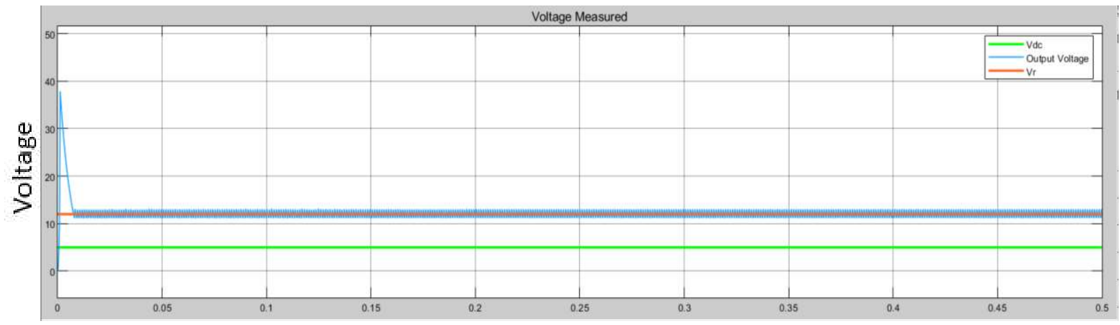

Figure 5.8: Boost converter with PI-controller (reference voltage 12V)

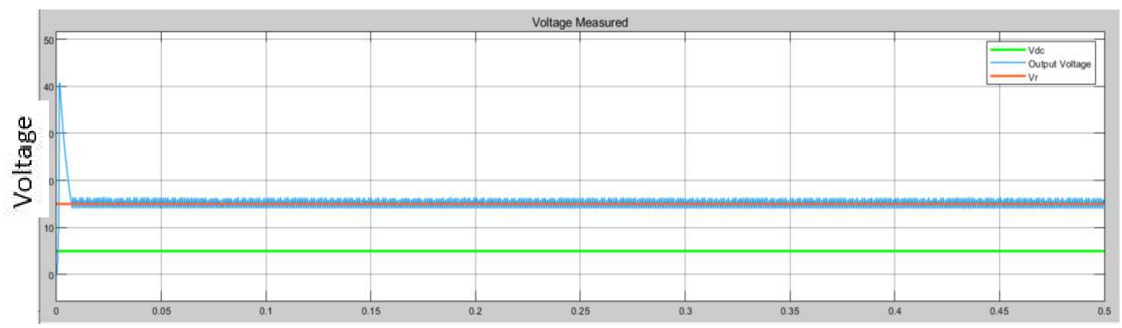

Figure 5.9: Boost converter with PI-controller (reference voltage 15V)

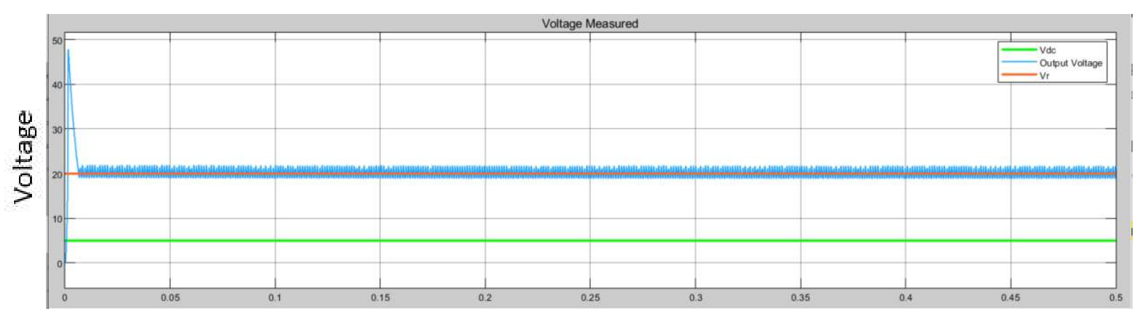

Figure 5.10: Boost converter with PI-controller (reference voltage 20V)

For the above converter with PI controller Fig 5.7, the zero of compensator is located at 10 and Proportional gain is (K_p) 5.

5.3.2 Buck Converter with PI controller

A buck converter steps down the input voltage to a lower output voltage. It is commonly used in applications where a lower voltage is required from a higher voltage source. The buck converter is efficient and can deliver high currents, making it suitable for various power supply applications. Table 5.15 shows the specification of Buck Converter chosen to design and simulate a PI controller technique discussed in this chapter.

Table 5.15: Buck converter parameters

Parameter	Value
Input DC Voltage	V_{dc} = 12 V
Inductance	L = 50µH
Capacitor	C = 220µF
Load resistor	R = 10Ω
Frequency	F = 40000 Hz

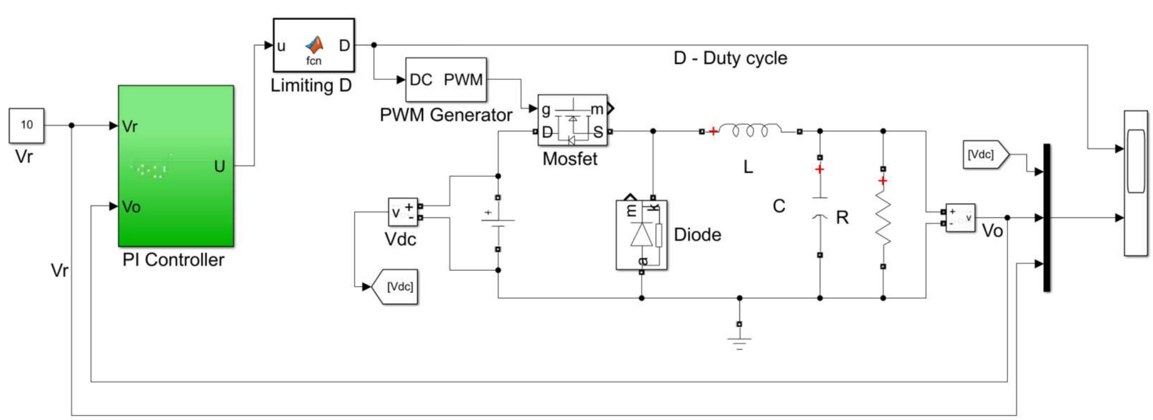

Figure 5.11: Buck converter with controller

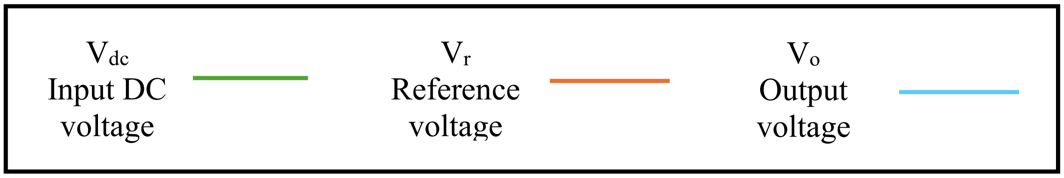

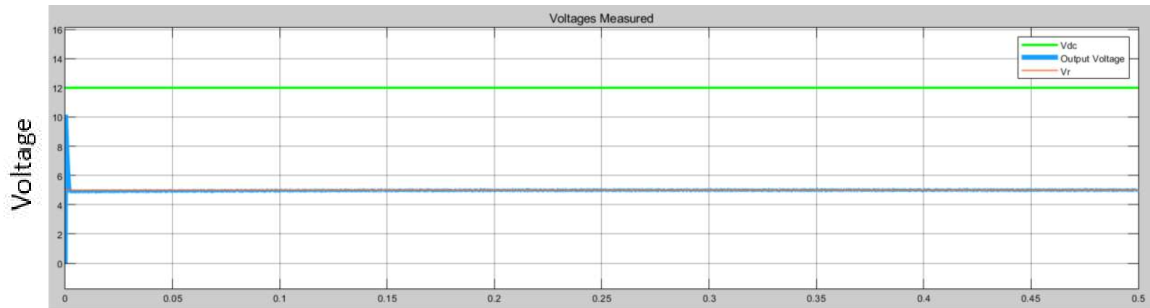

Figure 5.12: Buck converter with PI-controller (reference voltage 5V)

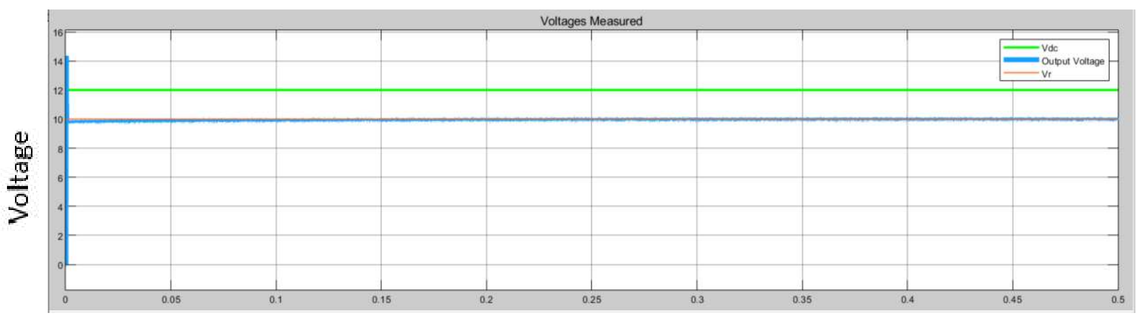

Figure 5.13: Buck converter with PI-controller (reference voltage 10V)

For the above converter with PI controller Fig 5.11, the zero of compensator is located at 10 and Proportional gain is (K_p) 5.

5.3.3 Buck-Boost Converter with PI controller

Table 5.16: Buck-Boost converter parameters

Parameter	**Value**
Input DC Voltage	V_{dc} = 12 V
Inductance	L = 50µH
Capacitor	C = 220µF
Load resistor	R = 10Ω
Frequency	F = 40000 Hz

A buck-boost converter is a type of DC-DC converter that can either step up (boost) or step down (buck) an input voltage to produce a desired output voltage. It combines the principles of both buck and boost converters, allowing it to handle input voltages that are either higher or lower than the desired output voltage. Requires more complex control circuitry compared to simple buck or boost converters. Table 5.16 shows the specification of Buck-Boost Converter chosen to design and simulate a PI controller technique discussed in this chapter.

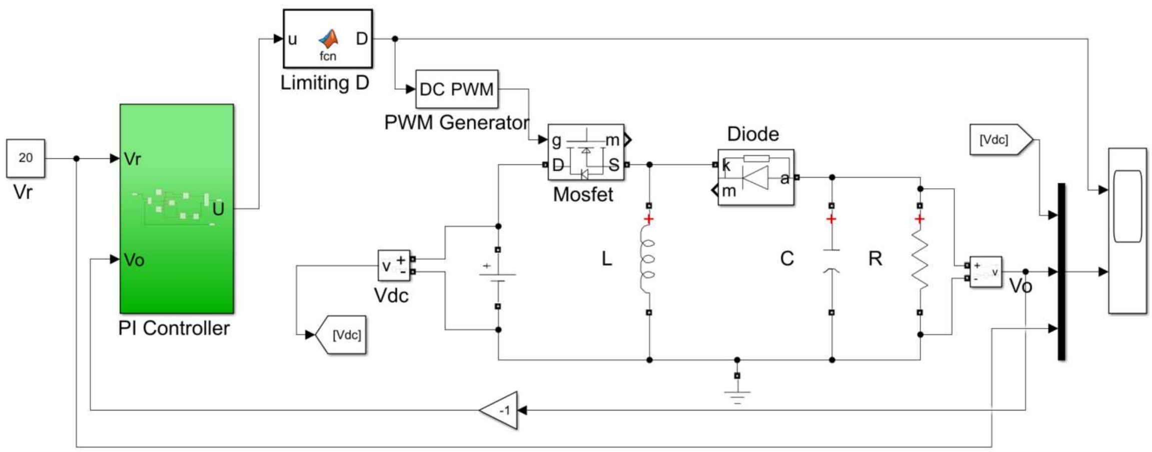

Figure 5.14: Buck-Boost converter with controller

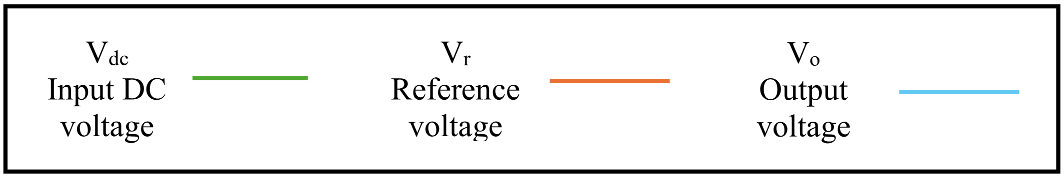

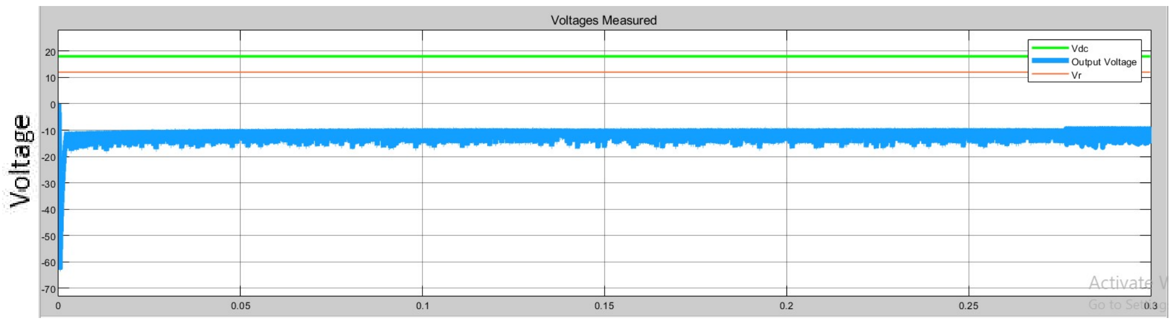

Figure 5.15: Buck-Boost converter with PI-controller (reference voltage 12V)

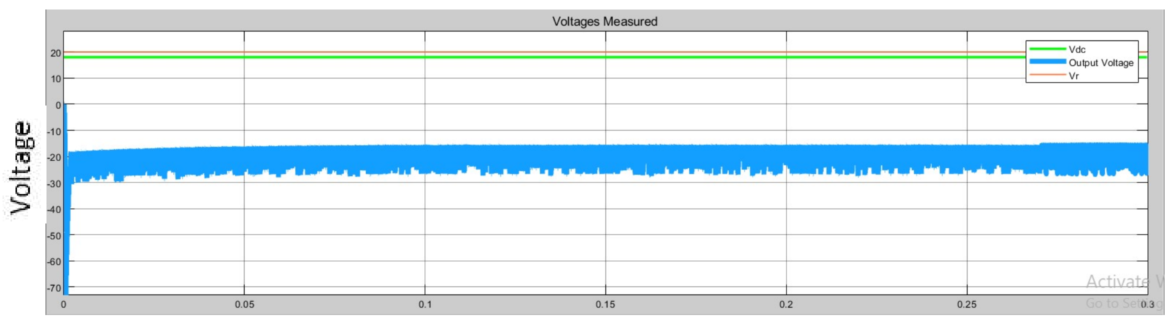

Figure 5.16: Buck-Boost converter with PI-controller (reference voltage 20V)

For the above converter with PI controller Fig 5.14, the zero of compensator is located at 10 and Proportional gain is (K_p) 5. And from the Fig 5.6-5.8, Fig 5.10-5.11 and Fig 5.14-5.15 it is evident that PI controller designed with $GK_p >> 1$ generated D and makes output voltage to follow the input reference voltage.

CHAPTER SIX

CONCLUSION AND FUTURE WORK

6.1 Conclusion

This dissertation presents comprehensive methods for analyzing and designing non-trivial control systems related to redundant input electric drives and highly variable gain converters. The key is to pose these challenges as feedback control problems for an uncertain interval, a significant departure from traditional methods.

The separately excited direct current motor (SEDCM), which has redundant field and armature voltages, was converted into an uncertain interval system by minimizing the armature current with the field voltage. Kharitonov stability criterion for interval systems and Root-Locus plots were employed to explain the stable region for the controller's proportional plus integral (PI) control gains. A direct adaptive controller was designed using the Lyapunov stability criterion, with the guidance of the parameter boundary.

Three classes of DC-DC converters, the buck, boost, and buck-boost, were also cast as uncertain interval systems with rapid-changing gains. The stability and feedback analysis and design were extended to these systems to yield robust closed-loop PI-controlled DC converters. The unified methodology produces near instantaneous and accurate tracking responses for the buck, boost, and buck-boost converter.

In conclusion, this dissertation presents a novel, comprehensive approach to understanding and controlled uncertain interval systems that can be applied to non-trivial problems related to electric drives. Theoretical and numerical examples were implemented and illustrated via the Matlab, Simulink, and Simscape platforms.

6.2 Future Work

Several potential future research directions can be explored based on the optimization and controller techniques discussed in this dissertation.

One possible area of future work is implementing adaptive controller design to ADAS features such as LKA, LC and Smooth steering etc. and comparing different adaptive control techniques. Another possible area of future work is extending the transfer function-based controller design technique to quadratic converters, tapped-inductor converters, LCCT converters and A-source converters.

Next possible area, the SEDC motor with optimization system and DC-DC converters with PI controller could be integrated with one another such that an electric drive system is built for electric vehicles. This would require more understanding of electronics, motors and control algorithms.

REFERENCES

[1] C. C. Chan, R. Zhang, K. T. Chau, J. Z. Jiang. “Optimal Efficiency Control of PM Hybrid Motor Drives for Electrical Vehicles”. Proceedings of the 28th Annual IEEE Power Electronics Specialists Conference, vol. 1, pp. 363–368, 1997.

[2] Iqbal Husain, “Electric and Hybrid Vehicles,” ISBN 978-1-198-59058 8(hbk), CRC Press, Edition. 3, pp. 189-192, 2005.

[3] S. Murtuza, N. Narasimhamurthi, S. T. Dilodovico. “DC Servo Control academic and Real.” Proceedings of the American Control Conference, IEEE Press, vol. 3, pp. 2036–2037, 1995.

[4] R. N. Danbury. ”Servomechanisms for Incremental Motion: Power Dissipation Considerations” . Mechatronics, vol. 4, no. 1, pp. 25–36, 1994.

[5] A. M. Trzynadlowski. “Energy Optimization of a Certain Class of Incremental Motion DC Drives.” IEEE Transactions on Industrial Electronics, vol. 35, no. 1, pp. 60–66, 1988.

[6] Argoun, M. B, “On the stability of low-order perturbed polynomials.”IEEE Transactions on Automatic Control, 35(2), pp.180–182, 1990.

[7] Bose, N. K., Jury, E. I., & Zeheb, E, “On robust Hurwitz Polynomials”. IEEE Transactions on Automatic Control, 33(12), pp. 1166–1168, 1988.

[8] Kharitonov, V. L, “Asymptotic stability of an equilibrium position of a family of system of linear differential equation Differential Equations,” 14(11), pp. 1483–1485, 1978.

[9] Nusret Tan, Ibrahim Kaya, Celaleddin Yeroglu, Derek P.Atherton, “Computation of stabilizing PI and PID controllers using stability boundary locus”, Energy Conversion and Management 47, Elsevier Energy Conversion & Management, PP. 3045-3058, 2006.

[10] Zhuang M, Atherton DP. “Automatic tuning of optimum PID controllers.” IEE Proc Part D, pp. 140:216–24, 1993.

[11] Astrom KJ, Hagglund T, “PID controllers: Theory, design, and tuning.” Instrument Society of America, 1995.

[12] Milan A. Sheta, Vivek Agarwal, Paluri S. V. Nataraj, “A New Energy Optimal Control Scheme for a Separately Excited DC Motor Based Incremental Motion Drive” International Journal of Automation and Computing, pp. 267-276, 2009.

[13] Jeerawan Homjan, Kongpol Areerak,Tidarut Areerak, Sasiya Udomsuk,Kongpan Areerak, "Energy saving for separately excited DCmotor via optimization method with deterministic recursive linear least squarealgorithm," Springer: Electrical Engineering, pp. 3955-3967, 2022.

[14] Ahmed Hussein, Kotaro Hirasawa, and Jinglu Hu,"A robust control method for a PV-supplied DC motor using universal learning networks," Solar Energy, vol. 76, issue 6, pp. 771-780, 2004.

[15] D. Kukolj, F. Kulic, and E. Levi, "Design of the speed controller for sensorless electric drives based on AI techniques: a comparative study," Artificial Intelligence in Eng., vol. 14, issue 2, Apr. 2000, pp.165-174.

[16] Jui-Hong Horng, "Neural adaptive tracking control of a DC motor," Information Sciences, 1-4 Sept. 1999, vol. 118, issues 1-4, pp. 1-13.

[17] C. Machbub, A. S. Prihatmanto, and Y. D. Cahaya,"Design and implementation of adaptive neural networks algorithm for DC motor speed control system using simple microcontroller," Proc. Of 2001 4th IEEE Intl. Conf. Power Electronics and Drive Systems, vol. 2, 22-25 Oct. 2001, pp. 479-483.

[18] Paul Krause, Oleg Wasynczuk, Scott Sudhoff, Steven Pekarek, "Analysis of Electric Machinery and Drive systems", ISBN 978-1-118-02429-4(cloth), IEEE press series on Power Engineering, 2013.

[19] Ying J. Huang, Yuan-Jay Wang, "Robust PID tuning strategy for uncertain plants based on the Kharitonov theorem," ISA Transactions 39, Elsevier, pp. 419-431, 2000.

[20] Isaac A Vitan, Victor Skormin, "Mathematical modeling, and computer simulation of a separately excited dc motor with independent Armature/Field Control", IEEE Transactions on industrial electronics, December 1990.

[21] Moley kutty George, "Speed Control of Separately Excited DC Motor", American Journal of Applied Sciences 2008.

[22] Karl J.Astrom, Bjorn Witternmark, "Adaptive Control".

[23] William L.Brogan, "Modern Control Theory".

[24] Fitzgerald & Kingsley's, "Electric Machinery".

[25] https://www.mathworks.com/help/ident/ref/tfest.html.

[26] Furkan Nur Deniz, “PID Control Systems Design for Second Order Model Approximation by Using Stability Boundary Locus Fitting”.

[27] Jitendra Sharma, Yogesh V. Hote, “PID Controller Design for Interval Load Frequency Control System with communication time delay”, Elsevier Control Engineering Practice 2019.

[28] Ying J. Huang, Yuan-Jay Wang, “Robust PID tuning Strategy for Uncertain plants based on the Kharitonov Theorem”, Elsevier ISA Transactions 2000.

[29] Marian K.Kazimierczuk, “Pulse-Width Modulated DC-DC Power Converters”.

[30] Ranya Badawi, “Enhancing Enumeration-Based Model Predictive Control for DC-DC Boost Converter with Event-Triggered Control”. European Control Conference 2022.

[31] Ranya Badawi, “Performance Evaluation of Event-Triggered Model Predictive Control for Boost Converter”, IEEE Vehicle Power, and Propulsion Conference 2022.

[32] Alejandro Garces-Ruiz, “Model Predictive Control with Stability Guarantee for Second-Order DC/DC Converters”. IEEE Transactions on Industrial Electronics 2023.

[33] Zhaoxia Leng, Qingfeng Liu, “A Simple Model Predictive Control for Buck Converter Operating in CCM”, IEEE 2017.

[34] Sandeep Kumar Soni, “Event-Triggered Control for DC-DC Boost Converters”, IEEE 2022.

[35] Zengin, Nursefa , et al. “Lyapunov Analysis of Least Squares Based Direct Adaptive Control.” IEEE 61st Conference on Decision and Control, Dec. 2022, pp. 709–714, https://doi.org/10.1109.

[36] Gani, Md. Maniurul, et al. “Modeling and Designing a Genetically Optimized PID Controller for Separately Excited DC Motor.” IEEE Xplore, Feb. 2019.

[37] F.L. Luo and H. Ye “Positive output cascade boost converters” IEE Proceedings Electrical, Sep 2004, Vol. 151, pp. 590-606.

[38] Munevver Mine Ozyetkin, “A simple tuning method of fractional order PI^{λ}-PD^{μ} controllers for time delay systems” ISA transactions, Vol. 74, Feb 2018, pp. 77-87.

[39] Cem Onat, "A new design method for PI-PD control of unstable processes with dead time" ISA transactions, Vol. 84, Oct 2018, pp. 69-81.

[40] Zheng Da,Ren Zhengyun,Fang Jian'an , Jiang Lei, "Computation of Stabilizing PI and PID Controllers by Using Kronecker Summation Method", Proceedings of the 27th Chinese Control Conference July 18, 2008, pp. 72-75.

[41] Supanna S. Kumar, Shreesha C. "Design of Robust PID Controller for a CSTR Plant with Interval Parametric Uncertainty using Kharitonov theorem" ICCPEIC-2016 IEEE, pp. 430-433.

[42] A Ferheen, M Chidambaram, "Design of robust PID controller for an interval plant", IEEE 2017.

[43] Serdal Atiç, Ibrahim Kaya, "Generalized Stability Boundary Locus for PI Controller Design for Controlling Integrating Processes with Dead Time"

[44] Danaboyina Srinivasa Rao, Mangipudi Siva Kumar, "New algorithm for the design of robust PI controller for plants with parametric uncertainty", Transactions of the Institute of Measurement and Control – 2017, pp 1-9.

[45] Ibrahim Kaya, Serdal Atiç, "PI Controller Design based on Generalized Stability Boundary Locus", ICSTCC 2016, Oct 2016, pp 24-28.

My Publications

[1] Narendra Kintali, Nashwan Sebi, and Professor Ka C Cheok, "*Optimization of Separately Excited DC motor Voltages using Minimization Technique and Discussion on Stability*," 37th International Electric Vehicle Symposium & Exhibition (EVS37), Coex, Seoul, Korea, April 23-26, 2024 – selected

[2] Nashwan Sebi, Narendra Kintali, and Professor Ka C Cheok, "*Rear-end Vehicle Collision Avoidance using Reinforcement Learning*," 39th International Conference on Computers and Their Applications (CATA 2024), New Orleans, Louisiana, USA March 18-19, 2024.

[3] Ka C Cheok, Ana Farhat, Sangeetha Prakasam & Narendra Kintali, "*Levenberg-Marquadt Algorithm tuned Gradient Descent-based Model Reference Adaptive Control Scheme*", Procs of Computer Applications in Industry and Engineering (CAINE) - 2016, Denver, Colorado, USA, pp 73-79, September 26-28, 2016.